



**HAL**  
open science

## Investigating physical and thermal interactions between lava and trees: the case of Kīlauea's July 1974 flow

Magdalena Oryaëlle Chevrel, Andrew J.L. J.L. Harris, Alexian Ajas, Jonas  
Biren, Lucia Gurioli, Laura Calabro

### ► To cite this version:

Magdalena Oryaëlle Chevrel, Andrew J.L. J.L. Harris, Alexian Ajas, Jonas Biren, Lucia Gurioli, et al.. Investigating physical and thermal interactions between lava and trees: the case of Kīlauea's July 1974 flow. *Bulletin of Volcanology*, 2019, 81 (2). hal-01980212

**HAL Id: hal-01980212**

**<https://hal.science/hal-01980212>**

Submitted on 14 Jan 2019

**HAL** is a multi-disciplinary open access archive for the deposit and dissemination of scientific research documents, whether they are published or not. The documents may come from teaching and research institutions in France or abroad, or from public or private research centers.

L'archive ouverte pluridisciplinaire **HAL**, est destinée au dépôt et à la diffusion de documents scientifiques de niveau recherche, publiés ou non, émanant des établissements d'enseignement et de recherche français ou étrangers, des laboratoires publics ou privés.

# Investigating physical and thermal interactions between lava and trees: The case of Kīlauea's July 1974 flow

Magdalena Oryaëlle Chevrel<sup>1</sup> • Andrew Harris<sup>1</sup> • Alexian Ajas<sup>1</sup> • Jonas Biren<sup>1</sup> • Lucia Gurioli<sup>1</sup> • Laura Calabro<sup>1</sup>

<sup>1</sup> Université Clermont Auvergne, CNRS, IRD, OPGC, Laboratoire Magmas et Volcans, F-63000 Clermont-Ferrand, France

## Abstract

To examine whether there was any physical or thermal interaction between trees and lava when a lava flow inundates a forest we studied the Kīlauea's July 1974 lava flow. We mapped the location of ~600 lava-trees and the lava type (pāhoehoe versus 'a'ā), and sampled an additional ten lava-trees for chemical and textural analysis to infer flow viscosity and dynamics. The emplacement event lasted 3.5 hours and markers on the outer surface of the lava-trees allowed us to define initial high effusion rate and velocity (~400 m<sup>3</sup>/s and 5–10 m/s) that then declined to 9 m<sup>3</sup>/s and 4 m/s during a waning phase. We find that lava passing through the forest underwent an initial cooling rate of 4 °C/km which increased to 10 °C/km late in the eruption. This is no different to cooling rates recorded at Kīlauea for tree-free cases. There thus appears to be no effect on cooling for this case. The lava-trees did, though, form a network of vertical cylinders obstacles and evidence for local diversion of flow lines are noticed. However, this varies with lava type, as almost no lava-trees form in 'a'ā. We find a relation between the percentage of 'a'ā and the number of lava-trees per hectare. The pāhoehoe–'a'ā transition for this flow occurs at a viscosity of 10<sup>3</sup> Pa s and this appears to be a threshold below which lava-trees can form so as to behave as a network of obstacles, and above which they cannot.

**Keywords:** Lava-tree, lava channel, cooling rate, viscosity, pāhoehoe–'a'ā transition

## 28 **Introduction**

29 Lava flow emplacement dynamics are controlled by extrinsic parameters (topography, nature  
30 of the substrate, effusion rate, total volume emitted) and intrinsic properties (composition,  
31 temperature, vesicularity, cooling rate) which together control the viscosity and velocity of  
32 the lava (e.g., Chevrel et al. 2013; Harris and Rowland, 2015; Kolzenburg et al. 2017; Rumpf  
33 et al. 2018). Under cooling-limited conditions (Pinkerton and Wilson 1988; Wilson and Head  
34 1994), the run-out distance of a lava flow (i.e., the maximum length that can be reached at a  
35 given effusion rate) has typically been related to the rate of effusion (Walker 1973), to the  
36 total volume of material erupted (Malin 1980) and to rheological changes due to the heat loss  
37 (Pinkerton and Wilson 1994). The evolution of the surface morphology of a channel-fed lava  
38 flow system commonly changes from a pāhoehoe-dominated proximal zone, to a medial tran-  
39 sition zone with the formation of lava channels, to a distal zone of ‘a’ā (Lipman and Banks  
40 1987). The transition between pāhoehoe and a’ā has been the focus of many studies and is  
41 thought to be caused by an increase in strain rate or by a change in lava rheological properties  
42 including higher viscosity, development of yield strength and disruption of the cooled surface  
43 (e.g., Peterson and Tilling 1980; Cashman et al. 1999; Sehlke et al. 2014). To characterise the  
44 changing properties that control lava down-flow behaviour, several techniques have been  
45 used. If the flow is active, lava properties may be directly measured in the field (Lipman and  
46 Banks 1987; Moore 1987; Crisp et al. 1994; James et al. 2007; Belousov and Belousova  
47 2018). In the case of solidified flows, several studies have analysed the textural and chemical  
48 evolution of samples collected between the vent and the flow front to obtain down-flow ther-  
49 mal, textural and rheological evolution (e.g., (Soule et al. 2004; Riker et al. 2009; Chevrel et  
50 al. 2013; Robert et al. 2014; Castruccio and Contreras 2016). Other studies have modelled  
51 lava flows as function of cooling either with analogue materials (e.g., Hulme 1974; Sakimoto

52 and Gregg 2001; Garel et al. 2014) or via numerical models (e.g., Crisp and Baloga 1994;  
53 Dragoni and Tallarico 1994; Harris and Rowland 2001; Bernabeu et al. 2016; Kelfoun and  
54 Vargas 2016).

55 The lava flow emplacement is also highly dependent on ground topography, substrate  
56 roughness (Rumpf et al. 2018) and encountered obstacles (Dietterich and Cashman 2014).  
57 Dietterich et al. (2015) examined how lava, using small basaltic flows created in the laborato-  
58 ry—effectively pouring molten basalt onto a synthetic topography— can be diverted by ob-  
59 stacles. Using the same method, Rumpf et al. (2018) showed that the higher the ground  
60 roughness the lower the flow front velocity. Computational simulations were also used by  
61 Chirico et al. (2009) and Scifoni et al. (2010) to examine the effect of barriers on flow paths.

62 However, the dynamics of lava moving through forested areas remains rather un-  
63 known. Recently, Bernabeu et al. (2018) showed that a fluid moving through a grid of vertical  
64 cylindrical obstacles, as analogue for a lava flow inundating a dense forest, would form a  
65 wider and thicker flow than expected. Besides when the lava enter in contact with trees, ener-  
66 gy will also be required to heat, dry and combust wood (e.g., Van Wagner 1967; Babrauskas  
67 2002). These studies suggest that the presence of cold, combustible obstacles in the flow may  
68 be added to the list of extrinsic parameters that potentially affect lava flows. Trees may thus  
69 play a role in both thermally and mechanically interacting with the flowing lava to exert a  
70 control on lava flow rheology, and thus also dynamics and morphology, as well as path and  
71 dimensions. However, although several studies exist that describe the morphology of casts left  
72 by trees due to the quenching effect on lava flowing around them, i.e., lava-trees (e.g., Finch  
73 1931; Moore and Richter 1962; Lockwood and Williams 1978; Carveni et al. 2011; Parcheta  
74 et al. 2012), no data are available on the effects of vegetation on lava flow propagation. There  
75 therefore remains an outstanding question: can trees cause enhanced lava cooling and me-  
76 chanically interact with an advancing flow, thereby playing a role in changing flow dynamics

77 and morphology (pāhoehoe versus ‘a‘ā) as compared with a forest-free scenario? To answer  
78 this question our study focuses on the July 19–22, 1974 lava flow of Kīlauea (Hawaii), a flow  
79 well-known for its abundance of standing lava-trees (Hazlett 1993). We carried out detailed  
80 mapping and analysis of glassy samples collected from the inside and outside surfaces of the  
81 lava-tree casts and extracted flow temperature, plus crystal and bubble concentrations at each  
82 sampled site. These results were then used to estimate down-flow cooling and infer the corre-  
83 sponding increase in viscosity, which—for this case—appears no different to a tree-free em-  
84 placement case. Our analysis does, however, imply that some local mechanical interactions do  
85 occur with lava-trees, and allows us to propose a conceptual model and a viscosity threshold  
86 at which a tree may or may not turn into a lava-tree, and hence can or cannot interact. This  
87 point corresponds with, but does not cause, the pāhoehoe–‘a‘ā transition.

#### 88 Lava-trees and tree-molds

89 It is well known that when low viscosity pāhoehoe invades a forest, often the lava does not  
90 topple the trees but rather cools rapidly against the cold, damp bark to form a cast of the tree  
91 (Finch 1931; Jaggar 1945; MacDonald et al. 1983). Following Finch (1931), a tree inundated  
92 by lava will form a quenched cast of lava around it. The tree will then heat to combustion and  
93 burn slowly as the lava continues to flow around it (Honda 1998). If the lava level remains  
94 constant then, once the tree has burnt away, a “hollow cylinder” (Moore and Richter 1962) or  
95 “hole” (Finch 1931) will be left in the lava flow with the same size and form as the tree root,  
96 trunk and branch system. The texture of the bark is often imprinted onto the interior of the  
97 cast surrounding the hole, so this is termed a “tree-mold” (Finch 1931; Lockwood and  
98 Williams 1978). If the lava level subsequently drops, then the tree cast will instead be left  
99 standing as a column (Fig.1); this is a “lava-tree” (Finch 1931; MacDonald et al. 1983;  
100 Lockwood and Hazlett 2010). In this case, rapid lowering of the lava level may cause the  
101 crust to scrape across the plastic outer surface of the cast to cause striations and tension-

102 produced gash fractures (Moore and Richter 1962). In some cases, the lava may entirely over-  
103 come the height of the tree to form a closed lava-tree (Moore and Richter 1962). Where the  
104 lava did not reach the top of the tree, the hole left by the consumed trunk is exposed forming  
105 an open lava-tree. In such a case, one can have access to pre-lava inundation ground surface  
106 through the shaft (Fig. 1). In some places, tree trunks inside the cast may not burn completely,  
107 indicating that the lava inundation and drainage must have taken place in a short time (Fiske  
108 and Koyanagi 1968); in others, the tree may be toppled and ingested horizontally into the lava  
109 or its crusts (basal or surface) to form horizontal, tubular molds (MacDonald et al. 1983;  
110 Carveni et al. 2011).

111 Lava-trees have been used in various ways, such as to estimate maximum thicknesses  
112 reached by a lava flow (Moore and Richter 1962; Moore and Kachadoorian 1980), to retrieve  
113 flow direction (Lockwood and Williams 1978), or to reconstruct the pre-eruption topography  
114 of the ground surface (Jones et al. 2017; Parcheta et al. 2012). Lava-trees have also been de-  
115 scribed as tools for “public educational purposes” (Carveni et al. 2011) and, given their nar-  
116 row cave-like properties, been the focus of speleological studies (Bella and Gaál 2007). Addi-  
117 tionally, charcoal left beneath a flow or in the tree molds (Searle 1958) can be analysed by  $C^{14}$   
118 for dating lava flow emplacement (Kuntz et al. 1986).

119 All of these studies have described the tree-lava contact and the formation or structure  
120 of tree molds and lava-trees. However, no in-depth study exists on under which conditions  
121 lava-trees form and whether and how a forest might influence the emplacement dynamics and  
122 final form of a lava flow. Guest et al. (1987), Harris et al. (2017) and Bernabeu et al. (2018)  
123 have suggested that trees can act to, or at least participate in, slowing down the advance of a  
124 lava flow. In addition, Lockwood and Williams (1978) have shown that if two trees are suffi-  
125 ciently close, a chilled crust may form between the trunks to form a wall or barrier of solid  
126 lava

127 The July 19, 1974 lava flow

128 Around 12:30 (Hawaiian Standard Time) on July 19, 1974, lava fountaining began from a  
129 small fissure at the base of the south wall of Keanakāko‘i pit crater; with a second fissure  
130 opening a few minutes later north of Keanakāko‘i (Lockwood et al. 1999). Shortly thereafter,  
131 two en-echelon fissures appeared on the south-eastern sector of the caldera floor, feeding a  
132 pāhoehoe sheet flow eastward and northward across the caldera floor (Lockwood et al. 1999).  
133 Around the same time, the fissures extended through the Ōhi‘a forest to the west of  
134 Keanakāko‘i to feed “a fast-moving fluid flow consisting of slabby pāhoehoe and ‘a‘ā that  
135 travelled quickly to the south and southeast” for a distance of 2 km (Lockwood et al. 1999).  
136 By 13:00, lava from these fissures began to cascade into Keanakāko‘i to the north and Lua  
137 Manu craters to the east, forming a second, eastern, lava flow unit and cutting the chain of  
138 craters road (Fig. 2). Although the eruption continued until July 22, activity along the fissures  
139 to the east of Keanakāko‘i ceased by 16:15 on July 19 (Lockwood et al. 1999), having lasted  
140 around three and a half hours. Soule et al. (2004) gives a volume for the south-eastern unit of  
141  $3.5 \times 10^6 \text{ m}^3$ , for a mean output rate (given a 3–5 hour eruption duration) of 195–325  $\text{m}^3/\text{s}$   
142 (280  $\text{m}^3/\text{s}$  for a 3.5 hour duration). It is the southeast lava flow of this fissure system on which  
143 we focus (Fig. 2).

144 This south-eastern lava flow formed a “field of lava-trees” (Lockwood et al. 1999),  
145 and Glatzer (1974) reports forest fires ignited by the passage of the lava, although these were  
146 “well under control by nightfall” on July 19. Instead, the “biggest headache” was “illegal  
147 parking (by sightseers) in the fire lanes”, where “every possible place to park” was filled  
148 (Glatzer 1974). The damage caused to forest in this region due to the 1959 eruption of Kīlauea  
149 Iki and the 1974 eruption, as well as subsequent regeneration, has since been studied by  
150 Smathers and Mueller-Dombois (2007). The south-eastern lava flow is also the same flow as  
151 the one studied by Moore and Kachadoorian (1980) and Soule et al. (2004). Moore and

152 Kachadoorian (1980) used the lava-trees to approximate the maximum flow depth and thereby  
153 obtained maximum average flow velocities — 1.56 m/s (near-vent) and 0.14 m/s (distally) —  
154 assuming a viscosity of around 2000 Pa s. Velocities and viscosities are also available from  
155 features of super-elevation for a lava channel active during this eruption to the north of  
156 Keanakāko‘i where lava “raced down a curving gully, with lava banking up against and spray-  
157 ing the outside of several bends” (Lockwood et al. 1999). In this channel, velocities were in  
158 excess of 8 m/s and viscosities were calculated by Heslop et al. (1989) as being 80–140 Pa s.  
159 In contrast, Soule et al. (2004) examined the pāhoehoe–‘a‘ā transition in the south-eastern  
160 flow, which they estimated occurred at a distance of 1.5 km from the vent. In the present  
161 work, we examine whether the presence of trees affected downflow cooling, and hence rheo-  
162 logical and dynamic changes in the channel-contained lava, as well as the relationship be-  
163 tween the presence of lava-trees and the pāhoehoe–‘a‘ā transition.

## 164 **Methods**

### 165 Mapping and sampling

166 The lava flow area, surface morphology and lava-tree locations were mapped using digital  
167 elevation model (DEM) with spatial resolution of 10 m and a vertical accuracy of 1–2 m, as  
168 derived from TOPSAR (topographic synthetic aperture radar) by Mougini-Mark and Garbeil  
169 (2005). The U.S. Geological Survey 7.5-minute (1:24,000-scale) topographic map sheet for  
170 the Kīlauea Crater quadrangle (1981 edition) was also used to support mapping, along with  
171 the cloud-free image satellite from GoogleEarth™ (image © 2018 DigitalGlobe –  
172 01/30/2016) in which individual lava-trees, as well as tree trunks lying on the flow surface,  
173 can be discerned. Locations of all lava-trees were added as a layer, and the density of lava-  
174 trees (number of lava-tree per unit area) was calculated from the number of objects within  
175 200-m-long sectors along the length of the flow. The number of trees per unit area before the

176 eruption was also estimated via counting treetops in areas of one hectare from an aerial image  
177 taken in 1965 (<https://guides.library.manoa.hawaii.edu/aerials/digital> - see online resource 1)  
178 and from an area aside of the flow using the GoogleEarth™ (image © 2018 DigitalGlobe –  
179 01/30/2016).

180         Additionally, field mapping and sampling were carried out in November 2016. During  
181 field work, 35 lava-trees within 200 m from the vent were located with hand-held GPS  
182 (WGS84) and their dimensions measured. Measured dimensions are marked on Fig. 1c and  
183 included: the diameter of the central hole, the width of the ring of solid lava surrounding the  
184 central hole, the height of the lava-tree above the current surface, and the depth of the central  
185 hole (i.e., distance from the highest flow level to the pre-existing ground surface). In addition,  
186 two sets of samples were collected. The first set corresponds to the sampling of nine lava-  
187 trees - one lava-tree every 200 m along a straight line in the centre of the channel between the  
188 vent and the flow front (T1–T9, Fig. 2 and 3, Table 1), plus one lava sample located on the  
189 eruptive fissure itself (vent sample “V” in Fig. 2). This set of samples is used to study the lava  
190 chemical and textural variation down flow. The sampling involved the whole width of the cast  
191 at the top of the lava-tree, so that the hand sample included the cast surface that was in contact  
192 with the tree (hereafter called “tree-side”) and the exterior of the cast that was in contact with  
193 the lava when it drained away (hereafter called “lava-side”). All dimensional measurements of  
194 Fig. 1c were also taken. Two to three thin sections were made from each lava-tree: one from  
195 the tree-side surface (hereafter labelled “-T”), a second from the lava-side surface (hereafter  
196 labelled “-L”), and—if possible—a third between the tree and lava sides (hereafter labelled “-  
197 M”), for a total of 26 thin sections (Fig. 3). The second set of samples was collected on the  
198 lava side of a single tree (T10, Fig. 4) to observe the lava chemical and textural evolution  
199 from the bottom to the top of the lava-tree cast. This lava-tree (T10) was selected as it was  
200 one of the tallest (1.92 m) found during the down-flow sampling, and showed six level mark-

201 ers where lava had remained at a stable level for a short period of time during waning flow.  
202 One sample was taken from each level (Fig. 4).

203 Chemical and textural analyses

204 The dense rock equivalent (DRE) density was determined from powdered sample fragments  
205 of known masses and using an Accupyc 1340 Helium Pycnometer that measured their vol-  
206 umes. The bulk density of the samples was measured using an envelope density analyser (Mi-  
207 cromeritics Geopyc 1360), which measures the difference in the volume of a quasi-fluid me-  
208 dium with and without the sample embedded in that medium. As presented by Kawabata et al.  
209 (2015) the Geopyc instrument can measure the envelope density of objects of different sizes  
210 and shapes. Prior to immersion, samples were dried in an oven for 24 hours at a temperature  
211 of 70 °C and then wrapped with thin laboratory parafilm®, to preserve external irregularities  
212 but to avoid the medium entering the porous sample. The standard deviation was estimated  
213 from five measurements to be  $\pm 30 \text{ kg/m}^3$  by Thivet (2016). The density-derived vesicularity  
214 was then calculated using the relationship given by Houghton and Wilson (1989).

215 Bulk rock major element analysis of one sample was carried out with Inductively Cou-  
216 pled Plasma – Atomic Emission Spectroscopy at the Laboratoire Magmas et Volcans (LMV,  
217 Université Clermont-Auvergne, France). The chemical composition of the glass and minerals  
218 were measured on polished thin sections via electronic microprobe CAMECA SX 100 (at 15  
219 kV and a defocused beam of 20  $\mu\text{m}$  at a current of 8 nA for glass and a focused beam at 15  
220 nA for minerals). The temperature of lava during emplacement was obtained using the glass  
221 composition through applying the MgO-glass geothermometer of Helz and Thornber (1987).  
222 Backscattered electron (BSE) images were collected by scanning electron microscopy (SEM)  
223 at magnifications of 25 $\times$  and 100 $\times$  and converted into binary images that were used for ex-  
224 traction of vesicle size distribution (VSD). Following Shea et al. (2010), we considered only  
225 vesicles that were larger than 10 pixels, which corresponds to an equivalent diameter of 0.05

226 mm. Crystal content in the glassy area of the thin section at the contact with the surface of the  
227 tree side and lava side was estimated using two images per sample via ImageJ, considering  
228 only crystals larger than three pixels; that is, greater in length than 6  $\mu\text{m}$ . The percentage of  
229 crystals was corrected for vesicularity and is therefore given for the vesicle-free mixture.

### 230 Estimation of lava viscosity and flow velocity

231 The viscosity of the three-phase lava mixture (fluid+crystals+bubbles) was estimated down  
232 the flow following the petrologic approach that considers the chemical, thermal and textural  
233 analyses of the samples (e.g., Pinkerton and Stevenson, 1992; Crisp et al. 1994; Guilbaud et  
234 al. 2007; Robert et al. 2014; Chevrel et al. 2013, 2018; Rhety et al. 2017). This method was  
235 applicable only to samples containing sufficiently large ( $>1 \text{ mm}^2$ ) areas of glassy matrix  
236 where the composition of the quenched melt could be measured, temperature calculated and  
237 crystal content extracted. First the viscosity of the interstitial melt was calculated as a function  
238 of chemistry and temperature using the model of Giordano et al. (2008). Second, the effect of  
239 the crystal cargo on viscosity was estimated following the method described in Mader et al.  
240 (2013), which uses the equation of Maron and Pierce (1956) and considering a crystal maxi-  
241 mum packing calculated using the average aspect ratio of the crystals (Mueller et al. 2010).  
242 We thereby obtained the vesicle-free mixture viscosity. Third, the effect of bubbles on the  
243 mixture viscosity was estimated from the vesicle fraction (obtained from the vesicularity de-  
244 rived from density) via the equation given by Llewellyn and Manga (2005) for deformable  
245 bubbles. Using these viscosities, we calculated the instantaneous velocity of the lava with the  
246 Jeffreys equation (Jeffreys 1925). For this, we considered the maximum and final depths of  
247 the flow as measured on each sampled lava-trees and an average underlying slope. Error  
248 propagation analyses on the estimation of lava viscosity and flow velocity are detailed in  
249 online resource 2.

## 250 **Results**

251 The July 19, 1974 lava flow and its lava-trees

252 We measured a length for the south-eastern lava flow of the July 19 flow field of 2200 m,  
253 with the unit covering an area of  $60.55 \times 10^4 \text{ m}^2$  in which a total of 598 lava-trees were  
254 mapped (Fig. 2). We note here that the flow generally contained lava-trees, and not tree-  
255 molds, indicating a flow-wide lowering of the flow level as the eruption progressed.

256 Morphologically, the flow can be divided into five zones (Fig. 2 and 5): near-vent  
257 pāhoehoe sheet flow, proximal channel, medial channel, distal channel and distal dispersed  
258 ‘a‘ā flow. Around the eruptive fissure, the lava is a smooth-surfaced “hummocky” (Swanson  
259 1973) pāhoehoe sheet flow over a surface with a slope of less than  $0.5^\circ$  (estimated from the  
260 lava flow surface). At 300 m from the fissure, multiple incipient channels arise within the  
261 pāhoehoe sheet flow. This is the zone of proximal channel which extends 200 m over a slope  
262 of  $1.9^\circ$  and feeds into the medial channel section at a distance of 500 m from the vent. Here,  
263 channels become well-formed across a zone of slightly steeper slopes ( $2.0^\circ$ ) and the flow be-  
264 comes concentrated in two 20–30 m-wide main channels. As noted by Soule et al. (2004),  
265 here the two channels bifurcate around a topographic high and form streams of ‘a‘ā and thin,  
266 broken slabs of pāhoehoe surrounded by low initial levees of pāhoehoe; the channel margin is  
267 commonly only marked by a line of shearing between the static levées and the moving lava  
268 stream. At a distance of 900 m, the two channels coalesce into a single, broad (~50 m wide)  
269 and 500 m-long stream of ‘a‘ā and pāhoehoe slabs between broad initial levees of the same  
270 material. Down this distal channel section the slope is  $0.75^\circ$  and, while the occurrence of co-  
271 herent pāhoehoe slabs within the channel decreases with distance, the percentage of surface  
272 area of ‘a‘ā increases (Fig. 2). After a distance of 1450 m, flow is of entirely ‘a‘ā. The zone of  
273 dispersed flow is 100 to 180 m wide, lies on a slope of  $1.1^\circ$  and feeds two 70–90 m-wide  
274 lobes with 2–3 m high flow fronts (Fig. 5).

275           Following Moore and Kachadoorian (1980), the thickness of the lava down flow was  
276 measured from the highest lava stand as given by the full lava-tree depth (i.e., value  $D$  in Fig.  
277 1c). Then, following Jones et al. (2017) the final, lowest level was obtained from subtracting  
278 the lava-tree height above the current surface from the full lava-tree depth (i.e., value  $F = D -$   
279  $H$  in Fig. 1c). In the near-vent zone, lava-tree depths were in the range 1.1–7.7 m, with a mean  
280 of 3.2 m and a standard deviation of 1.3 m—this being the maximum flow level around the  
281 vent. Heights above the 1974 surface were between 0.42 and 1.95 m ( $1.1 \pm 0.4$  m), giving a  
282 final lava level of 0.5–6.5 m ( $2.1 \pm 1.1$  m). Down-flow, there was no systematic variation in  
283 lava level (Fig. 3). However, maximum levels ( $1.8\text{--}5.1$  m,  $1.9 \pm 0.7$ ,  $n. = 10$ ), as well as min-  
284 imum flow levels ( $0.2\text{--}2.4$  m,  $1.2 \pm 0.7$  m,  $n. = 10$ ), were generally lower than around the  
285 vent. These values compare with the maximum flow thicknesses of Moore and Kachadoorian  
286 (1980) of  $2.0\text{--}5.2$  m ( $3.8 \pm 1.1$  m,  $n. = 6$ ), and minimum thicknesses of  $1.1\text{--}1.7$  m ( $1.3 \pm 0.2$   
287 m).

288           In terms of lava-tree density (Fig. 6), the proximal part of the lava flow contains the  
289 highest concentration (20-30 lava-trees/ha), with more than half of the lava-trees being locat-  
290 ed in the first 400 m near the vent (25% of the flow area) where pāhoehoe sheet flow domi-  
291 nated. As distance increases from the zone of pāhoehoe sheet flow, the density of lava-trees  
292 steadily decreases as the proportion of ‘a‘ā to pāhoehoe increases (Fig. 6). There is a complete  
293 absence of lava-trees at the flow front, where ‘a‘ā is 100 %; and the last lava-tree is found 200  
294 m from the front. At the flow front, trees in the process of being bulldozed can be found top-  
295 pled onto the flow surface.

## 296 Morphology and dimensions of lava-trees

297 Near the vent and in the zone of pāhoehoe-sheet flow the lava-trees are, for the most part, well  
298 preserved. Most have conserved the initial tree trunk disposition of main trunk and branch  
299 systems and are lava-trees “en bouquet”; that is, they form a tightly grouped but upward

300 splaying system of trunks and branches (Fig. 7a). Others are lone standing pillars either closed  
301 (Fig. 7b) or open (Fig. 7c) and are associated with the remnant (unburnt) trunks of the trees  
302 responsible for the casts (Fig. 7c). The heights of the lava-trees measured from the pre-flow  
303 surface to their top are between 1.1–7.7 m (in average  $3.2 \pm 1.2$  m, n. = 42) and their casts  
304 have widths in the range 4–20 cm ( $10.12 \pm 3.12$  cm), with central hole (trunk) diameters of 6–  
305 70 cm ( $23 \pm 11.5$  cm). On the tree side of the cast the surface is smooth and tree bark imprints  
306 are well preserved. The lava side is rough, often with tension gashes, sharks teeth and stria-  
307 tions that can be tied to descending slabs of pāhoehoe (Fig. 7d). All of these features indicate  
308 that the outer surface of the cast was still sufficiently plastic to “take the impressions of the  
309 crust” (Moore and Richter, 1962) and to deform plastically (Nichols 1939). The descending  
310 pāhoehoe slabs remain in-place, surrounding the base of the lava-tree and uptilted towards the  
311 lava-tree and often forming a dome like structure around the lava-tree (Fig. 7e).

312 Lava accretion on the up-flow side of lava-trees and on the lava side of the casts was  
313 also often observed. The lava-tree of Fig. 4 is a good example. It is 1.9 m high, has a perime-  
314 ter of 2.1 m, and is capped by a 20-cm-wide ring of rough-surfaced glassy pāhoehoe blebs,  
315 and has five level markers down the lava side of the cast. These markers are expressed as  
316 aligned trains of glassy globules and up-flow accretions. Glassy globules are stretched down  
317 flow ( $150^\circ$  ESE) and plunge downwards at  $22\text{--}25^\circ$ . This is much steeper than the ground  
318 slope ( $2^\circ$ ), indicating rapid drainage in the down-flow direction. Up-flow accretions consist of  
319 larger blebs of rough surfaced pāhoehoe that wrap around the cast in the down flow direction,  
320 and have the same orientation and plunge as the trains of glassy globules (Fig. 4). This attests  
321 to maintenance of the high stand for a period of time to build the accreted cap, followed by a  
322 rapid decline in flow level with a series of brief stands at a single level to build the train-and-  
323 accretion sets. Given the 3-5 hour duration of the eruption, the total time for this process can

324 be no more than an hour or two and with the transient declines and pauses being of the time  
325 scale of minutes.

326 In some places lava-trees are grouped (Fig. 7f) including two to four trees located at 1  
327 to 2 meters of each other. In such a case, lava-tree casts merge to form a wall-like or barrier-  
328 like structure which can be aligned up or cross-flow (Fig. 7f). Their profiles are irregular with  
329 high points, marking the lava-trees, joined by lower ridges or “seams” (Lockwood and  
330 Williams 1978) of accreted lava that join the lava-tree group together.

331 Textural and thermal analyses

332 The texture of the rock is porphyritic with phenocrysts of olivine within a glassy to microcrys-  
333 talline matrix. Phenocryst content is 3 vol.% and does not change down flow. Microlites (<0.2  
334 mm) include olivine and plagioclase, and their content increases from 0.6 vol.% near the vent  
335 to 33.1 vol.% near the front (Fig. 8 and 9, Table 2). This gives a crystallization rate of around  
336 15 vol.% per kilometre. As shown by the detailed sampling of the lava-side cast of T10, the  
337 microlite content appears to increase from 12 vol.% at the top of the lava-tree to 25 vol.% at  
338 the bottom (Table 3; Fig. 4).

339 Density and vesicularity derived from density (using a DRE density of 3030 kg/m<sup>3</sup>)  
340 were in the range 1500–2000 kg/m<sup>3</sup> and 34-53 vol. %, respectively (Table 2, Fig. 10a). Only  
341 the sample from the tree side of T9 (near the vent) is markedly different with a density of 760  
342 kg/m<sup>3</sup> and a vesicularity of 75 vol.%, representing at-vent gas-rich lava. Thereafter, there is no  
343 down-flow trend in vesicle content (Fig. 10a), but vesicularity of the lava next to the tree is  
344 always greater than that in the middle of the cast, attesting to a decrease in the bubble content  
345 of the erupted (and flowing) lava with time. The VSD analyses reveal that most samples con-  
346 tain one vesicle population between 0.05 and 5 mm, except T5-T that also comprises some  
347 vesicles larger than 10 mm and T1-T that includes two populations (Fig. 10b).

348 The chemical composition of the glassy matrix (online resource 3) decreases down  
349 flow from an Mg# of 36 at the vent to 28 near the flow front (at 1.9 km). For the tree side, this  
350 decrease in Mg# translates to cooling from  $1139 \pm 2$  °C at the vent and  $1132 \pm 5$  °C at 1.9 km.  
351 For the lava side, we calculated cooling from  $1140 \pm 2$  °C to  $1118 \pm 13$  °C. The temperature  
352 decline estimated from the quenched lava against the tree is different to that for the lava side,  
353 where there is a cooling rate of 4 °C/km for initial lava quenched to the tree, and 10 °C/km for  
354 late-stage lava accreted to the outer portion of the cast (Fig. 9). These straddle the average  
355 cooling rate of 6 °C/km given for the same flow by Soule et al. (2004) but show a lower cool-  
356 ing rate during initial flow than during late-stage flow. From the sampling of the lava-side  
357 cast of T10, we see that the temperature may change by 2 °C from level to level, but there was  
358 no systematic variation with depth during drainage (Table 3, Fig. 4).

#### 359 Flow dynamics

360 The viscosity of the melt phase varies down flow as glass composition evolves and tempera-  
361 ture decreases, so that the melt viscosity increases from 470 Pa s at the vent to 700 Pa s distal-  
362 ly. Including the effect of the crystal fraction and deformable bubbles (Table 4), the viscosity  
363 of the three-phase mixture was estimated at 90-190 Pa s near the vent (considering the condi-  
364 tions at T9: 1140 °C, 3.6–13.5 vol.% crystals and 46-75 vol.% elongated bubbles). These vis-  
365 cosities are in-line with those of Heslop et al. (1989) estimated from the super-elevation fea-  
366 tures in the near-vent channel active to the north of Keanakāko‘i at the same time. Distally,  
367 the three-phase viscosity is up to 3600 Pa s (considering the conditions at T1: 1132 °C, 36  
368 vol.% crystals and 50 vol.% bubbles). Our results give a viscosity ( $\eta$  in Pa s) with distance  
369 (Dist in m) trend of  $\eta = 160e^{0.0017\text{Dist}}$  with an  $R^2$  of 0.94 (Fig. 11a).

370 This viscosity variation has a direct influence on the flow velocity (Fig. 11). At vent, at  
371 peak flow (maximum depth) velocities were as high as  $9.8 \pm 2.6$  m/s (Table 4); similar to the  
372 maximum velocities obtained by Heslop et al. (1989) but higher than what estimated by

373 Moore and Kachadoorian (1980). With distance down flow, the increase in viscosity causes  
374 the velocity to fall to  $0.3 \pm 0.2$  m/s at 1915 m. Declining output rate caused decreasing flow  
375 levels, so that the typical depth of late-stage flow near-vent ( $1.2 \pm 0.7$  m) gives a lower final  
376 velocity of 0.2-4 m/s at vent, waning to 0.04 m/s at 1915 m (Table 4). Given channel width of  
377 30m, the maximum flow depth and the final flow level measured at T5, this translates to a  
378 decrease in effusion rate from  $403 \pm 250$  m<sup>3</sup>/s to  $15 \pm 9$  m<sup>3</sup>/s.

## 379 **Discussion**

### 380 Cooling effects of a forest

381 The 19 July 1974 lava flows advanced through a montane dry forest typical of Kīlauea's  
382 vegetation SW of Keanakāko'i crater (Pratt and Gon III 1998). This zone receives less than  
383 1000 mm of rain per year and experiences a dry season between mid-May and mid-October  
384 when rainfall is less than 100 mm/month (Smathers and Mueller-Dombois 2007). The domi-  
385 nant forest tree is the Ōhi'a (Pratt and Gon III 1998), a pioneer species native to Hawaii that  
386 forms "the canopy for virtually all Hawaiian forests" (Lincoln 2009). All lava-trees identified  
387 in this study were of Ōhi'a. In the zone where the fissures feeding the south-eastern flow of  
388 the 19 July eruptive activity broke out, we estimated the number of trees before the eruption at  
389 55 to 95 per hectare. Giving the average trunk radii of 10.5 cm and a typical depth of 3.2 m,  
390 this gives an area of 2.1 m<sup>2</sup> of cold bark and a volume of 11 m<sup>3</sup> of wood available to interact  
391 with the molten lava. The question is: are such tree densities, lava-tree contact areas and wood  
392 volumes sufficient to contribute a cooling effect to lava moving through the forest?

393 Lava flowing through the forest underwent an initial cooling rate of 4 °C/km which in-  
394 creased to 10 °C/km late in the eruption. This compares with cooling rates of 7 °C/km esti-  
395 mated for this same lava flow by Soule et al. (2004) and for other lava flowing down channels  
396 in tree-free environments on Kīlauea and Mauna Loa (Crisp et al. 1994; Cashman et al. 1999;

397 Riker et al. 2009; Robert et al. 2014). Thus, the cooling rates appear normal, so there was no  
398 discernible enhanced cooling effect due to the forest. The increase in cooling rate between the  
399 beginning and end of the eruption was likely due to the decrease in velocity in the channels  
400 with time as output rate feeding the channel system, and flow levels in the channels, declined.  
401 Following Keszthelyi and Self (1998), a lower velocity flow will undergo a higher rate of  
402 cooling per unit distance than a higher velocity flow. Simply, there is more time for lava mov-  
403 ing at low velocity to cool as it passes from one location to the next than if it is moving at  
404 higher speed (Harris and Rowland 2009). In our case, the increase in cooling rate is consistent  
405 with a decrease in velocity in the proximal section (Tables 3 and 4).

406         The lack of a significant thermal interaction between the flowing lava and the trees,  
407 and hence no enhanced cooling effect, could be due to three reasons. First, the casts would  
408 have formed almost immediately and, as is the case for a tube roof (Keszthelyi 1995), would  
409 have provided excellent thermal insulation to the lava flowing around the tree and thereby  
410 isolating the tree from lava flowing down the channel. Second, the velocity of the lava (2–10  
411 m/s) and the small tree diameter (typically 0.2 m) would have meant that the flowing lava  
412 would have had a short interaction time (less than a tenth of a second) with the tree. Third, the  
413 forest had suffered damage due to fall-out during the Kīlauea Iki eruption of 1959 so that, as  
414 of 1962, the forest consisted of damaged Ōhi'a trees undergoing re-foliation, and lacked  
415 dense, mature undergrowth (Smathers and Mueller-Dombois 2007). This, coupled with the  
416 fact that the eruption occurred during the middle of the dry season, would have meant that the  
417 moisture loads and vegetation densities would not have been as high as in a mature, undam-  
418 aged forest. In the wet forest type that characterises the eastern edge of the flow and most of  
419 Kīlauea's east rift zone (Pratt and Gon III 1998), vegetation and water would have been more  
420 abundant still. Following Pratt and Gon III (1998), such zones consist of a closed-canopy (i.e.,  
421 high density) of Ōhi'a with an understory of dense tree fern. The dominant fern is the Ciboti-

422 um species (Pratt and Gon III 1998), notably Hapu'u which can reach heights of 6–9 m, has  
423 “loose, fibrous bark on their trunks” (Lincoln 2009) and large (2–4 m long) ponds (Merlin  
424 2005) which are loaded with water. Finally, locally, trees quenched the lava to solidify a zone  
425 of lava typically 10 cm wide. Considering the typical lava-tree height of 3.2 m, the quenched  
426 lava volume is  $0.3 \text{ m}^3$  per tree, and around  $180 \text{ m}^3$  within the flow. This volume is therefore  
427 rather small in comparison to the volume of the entire flow ( $3.5 \times 10^6 \text{ m}^3$ ).

#### 428 Mechanical interactions

429 The initial solidification of lava around the trees formed numerous lava-trees which remained  
430 in place as vertical pillars and provided a series of obstacles around which the lava had to  
431 pass. In the pāhoehoe sheet area of the flow, within 250 m of the fissure, about half of the  
432 trees have been changed into lava-trees, while further down flow, where the lava is of a'ā  
433 type, the lava destroyed all of the trees without creating any lava-trees.

434 Direction markers on the lava-side of the casts (Lockwood and Williams 1978) show  
435 that lava did have to move around each lava-tree. Three cases of diversion can be identified  
436 (Fig. 12): scattered (isolated), cross-flow grouped, and down-flow grouped. In the isolated  
437 case, there is an exceedingly local effect where flow paths diverge around the pillar-like ob-  
438 stacle which is just 0.06–0.6 m wide. In the case of the cross-flow grouped lava-trees, we  
439 have a barrier that can be up to 5 m wide (Fig. 7f). This impedes flow, causing flow to move  
440 laterally as well as to back up behind the barrier to build accretions that pile up on the up-flow  
441 side of the barrier. In the down-flow grouped case, a similar barrier to that formed in the  
442 cross-flow case is formed, but because of its down-flow alignment it has less effect on flow  
443 lines. However, the effect on diverging flow lines is greater than in the scattered case because  
444 enhanced accretion around the lava-tree group causes the obstacle to be wider (1–2 m) than in  
445 the case of an isolated lava-tree.

446           According to Dietterich et al. (2015), the velocity of the lava is halved after passing by  
447 an obstacle. It therefore seems that although we find the trees did not affect thermally the la-  
448 va, the lava-trees, once formed, act as a network of solid pillars or obstacles around which the  
449 flow must move. Following Bernabeu et al. (2018) this can be viewed as a porous medium  
450 through which the fluid must move. The greater the number of lava-trees, the lower the poros-  
451 ity and hence the greater the effect on the dynamics for the fluid moving through the obstacle  
452 network. High obstacle densities cause the flow to be impeded and delayed, with the shape of  
453 the flow being changed (over the obstacle-free case), where fluid will spread and pile up in  
454 the porous zone (Bernabeu et al. 2018). Thus, a lava flow moving through a forest should be  
455 wider, thicker and shorter than for the same flow moving over a tree-free surface. This is also  
456 in agreement with previous observation of lava flows being thicker and slower where they  
457 branch or encounter obstacles (Dietterich and Cashman 2014). This effect on lava flow ad-  
458 vance could also be compared with the recent study of Rumpf et al. (2018) where they find  
459 that flow front velocities are lower on rough terrain. However, they suggested that the slower  
460 advance rate is due to enhanced cooling through the higher surface contact area of an irregular  
461 substrate. Here we suggest that the thermal effect caused by the contact with the trees might  
462 be rather trivial and that the mechanical effect caused by vertical obstacles might be the main  
463 factor affecting the flow advances rate.

464           Interaction of lava with a forest might therefore affect lava flow hazard assessment be-  
465 cause of the potential mechanical effect of the trees once turned into lava-trees. Following  
466 Bernabeu et al. (2018), further modelling is necessary to quantify the effect of vertical pillars  
467 as local lava diverter or flow delaying mechanism. As argued by Dietterich et al. (2015), “mit-  
468 igation of lava-flow hazards must incorporate the dynamics of lava flow–obstacle interactions  
469 into barrier design”. To go further, we suggest here that once and if the trees have been suc-  
470 cessfully transform into lava-trees, they may play the role of a “leaky” barrier (Dietterich and

471 Cashman 2014). Growing well-designed forests between potential source vents and vulnera-  
472 ble infrastructure may therefore offer a way to mitigate the risk caused by low viscosity lava  
473 flows. However, experiments should be carried out to test if and how a dense forest would  
474 affectively split the flow and slow down the advance. Scenarios including various types of  
475 trees and different tree arrangements need to be designed and tested.

#### 476 Lava-trees and the pāhoehoe-‘a‘ā transition

477 There is a progressive down-flow transition from pāhoehoe to ‘a‘ā, beginning at a distance of  
478 400–500 m from the vent, and is complete by a distance of 1500 m (Fig. 6). This is consistent  
479 with the findings of Soule et al. (2004) who found the pāhoehoe-‘a‘ā transition occurring in  
480 this flow between 500 m and 1500 m. Soule et al. (2004) ascribed the transition to crystallini-  
481 ty, with ‘a‘ā formation initiating when a critical crystallinity of 18 vol.% was reached. Like-  
482 wise, we find that this transition initiates at 15–20 vol. %, which is the typical crystallinity  
483 between 400 m and 1000 m (Fig. 9), and a viscosity of  $10^3$  Pa s (Fig. 11).

484 We also find a coincidence between the incidence of lava-tree formation and the  
485 pāhoehoe-‘a‘ā transition which progressively declines from 20–30 lava-trees per hectare in  
486 pure pāhoehoe to zero in pure ‘a‘ā (Fig. 6). However, this is the pāhoehoe-‘a‘ā transition in-  
487 fluencing the process of tree-formation; and not vice-versa. Simply, fluid pāhoehoe can flow  
488 between trees without toppling them, quenching to their trunks to allow lava-tree formation.  
489 In contrast, ‘a‘ā bulldozes trees (as seen from the back-toppling cases at the flow front)  
490 knocking them down so that they do not remain as vertical structures around which the lava  
491 has to flow (Fig. 12). Thus, lava-tree formation (and flow impediment) is precluded. Instead,  
492 trees topple onto the flow to be rafted down flow to eventually be heated and burnt on the  
493 flow surface or rolled along in the basal clinker (Fig. 12). Thus, as lava progressively transi-  
494 tions to ‘a‘ā the incidence of lava-trees progressively declines. This decline follows a linear  
495 relationship whereby the number of lava-trees of per hectare (NT) is related to the percentage

496 of lava as pāhoehoe (AA) through  $NT = -0.17(AA) + 17$  ( $R^2 = 0.7$ ). Considering that the  
497 number of pre-existing tree per hectare is constant, this means that in the pāhoehoe sheet area  
498 of the flow, within the 150 m from the fissure, nearly all the trees have been changed into  
499 lava-trees, while further down flow, where the lava is of a'ā type, all of the trees have been  
500 destroyed.

501 Re-creating the emission history from a single lava-tree

502 Using the level markers on lava-tree T10 we can recreate the emplacement history of the lava  
503 flow. Initial flow entered the channel (17.5 m wide) in which T10 resided at an effusion rate  
504 of  $305 \text{ m}^3/\text{s}$  (Table 3). This is 75 % of the value obtained for the single master channel at 920  
505 m and into which this channel feeds (Table 4). Waning levels of flow in the channel reflected  
506 waning velocity and effusion rate, which dropped to a final value of  $7 \text{ m}^3/\text{s}$ . This is now  
507 around 50 % of the value obtained for the master channel at the end of the eruption at 920 m.  
508 Thus, it appears, the channel branch in which T10 resided took between 50 and 75 % of the  
509 total lava flux.

510 The distribution of effusion rate ( $E_r$ ) with lava depth ( $D$ ) shown in Table 3 has an ex-  
511 ponential decaying form ( $E_r = 1.4e^{1.87 D}$ ,  $R^2 = 0.97$ ). If we distribute these effusion rates  
512 through time to fit to the total erupted volume ( $3.5 \times 10^6 \text{ m}^3$ ) and eruption duration (3.5 hours)  
513 this gives a function for the duration at which each level (#) was maintained of duration  
514  $= 3.5e^{-693\#}$ . If we distribute the volume through time using this function we obtain the tim-  
515 ings shown in Table 5. These timings suggest that peak flow was maintained the first half of  
516 the 3.5 hour-long eruptive period, with waning emission occurring over the second half. Dur-  
517 ing waning, flow level (lava thickness) was maintained for an increasingly short period of  
518 time with shut down being abrupt. This is consistent with the observation by Lockwood et al.  
519 (1999) that “discharge rates at all fissures gradually began to decline” from around 2 hours

520 after the eruption began, with all activity having ceased another one hour and 40 minutes lat-  
521 er.

## 522 **Conclusion**

523 We studied the relationship between lava flow dynamics and lava-tree formation for the case  
524 of the July 19, 1974 lava flow of Kīlauea. We mapped the lava flow morphology (pāhoehoe  
525 vs. ‘a‘ā) and the distribution of lava-trees along the flow path. We found that lava-trees are  
526 abundant (>20 lava-trees/ha) in the pāhoehoe area but sparse (<5 lava-trees/ha) in the ‘a‘ā  
527 section of the flow. We conclude that lava-trees can be formed when the lava flow is fluid  
528 enough; in such a regime lava-trees can form in spite of high flow velocities (~10 m/s). How-  
529 ever, when the lava becomes too viscous, a living tree will be overridden and no lava-tree can  
530 be formed. This threshold occurs at a crystallinity of 15–20 vol% and viscosity of  $10^3$  Pa s  
531 where the pāhoehoe-‘a‘ā transition takes place so that trees begin to be bulldozed by the ‘a‘ā  
532 flow rather than flooded by pāhoehoe lava. If lava-trees form, markers on their outer surface  
533 allow the eruption history to be recreated, which in this case involved 1.5 hours of high effu-  
534 sion rate flow (at ~400 m<sup>3</sup>/s) followed by 1.5 hours of waning flow and abrupt shutdown.

535 In this case, no enhanced cooling effect due to the presence of the trees was recorded,  
536 but this may be a function of the rapidity of the inundation and the type of vegetation, which  
537 was in poor health at the time of inundation. Mechanically, though, the lava was locally di-  
538 verted by the array of solid cylinders formed by the lava-trees. Forests may thus have an ef-  
539 fect in delaying flow advance and may be able to locally divert a flow from the expected path.  
540 Further study on the effect of trees depending on their type will permit definition as to wheth-  
541 er tree stands of certain types could be used, once turned into lava-trees, as local lava diverter  
542 or flow delaying mechanism. Note, though, that if the lava is more viscous than a critical

543 threshold, that is here given at  $10^3$  Pa s, lava-trees will not form. Further work in this direction  
544 is clearly needed to assess the potential for vegetation barriers as a mitigation tool.

545

#### 546 **Acknowledgements**

547 The authors gratefully acknowledge the support of Matthew Patrick, the Hawaiian Volcano Observa-  
548 tory and Hawaiian Volcanoes National Park where work was completed under National park permit  
549 HAVO-2016-SCI-0064. The pole technique of LMV (Christophe Constantin, Jean-Luc Devidal, Jean-  
550 Marc Henot, Mhammed Benbakkar and Claire Fonquernie) is acknowledged for sample preparation  
551 and sam- ple analyses. Fieldwork was performed with the help of Scott Rowland and Alejandra Go-  
552 mez-Ulla who are greatly acknowledged. Additionally, we thank Taeko Jane Takahashi at the HVO  
553 library for helping us track down the internal and newspaper reports for the events of 19 July 1974.  
554 Finally, T. Gregg, A. Soule (reviewers) and H. Dietterich (editor) are greatly acknowledged for their  
555 thorough reviews and comments, which improved the quality of this work.

#### 556 **Funding information**

557 This research was financed by the Agence National de la Recherche through the project LAVA (Pro-  
558 gram: DS0902 2016; Project: ANR-16 CE39-0009, <http://www.agence-nationale-recherche.fr/Projet-ANR-16-CE39-0009>). This is ANR-LAVA contribution no. 7. Fieldwork was supported by the Labo-  
559 ratory of Excellence ClerVolc pro- gram 6, contribution no. 316. MOC acknowledges the Auvergne  
560 fellow-ship for support.  
561

#### 562 **References**

- 563 Babrauskas V (2002) Ignition of wood: a review of the state of the art. *J Fire Prot Eng* 12:163–189.  
564 <https://doi.org/10.1177/10423910260620482>
- 565 Bella P, Gaál L (2007) Tree mould caves within the framework of cave genetic classification. *Nat*  
566 *Conserv* 63:7–11
- 567 Belousov A, Belousova M (2018) Dynamics and viscosity of ‘a’ā and pāhoehoe lava flows of the  
568 2012–2013 eruption of Tolbachik volca- no, Kamchatka (Russia). *Bull Volcanol* 80:.  
569 <https://doi.org/10.1007/s00445-017-1180-2>
- 570 Bernabeu N, Saramito P, Harris AJL (2018) Laminar shallow viscoplastic fluid flowing through an  
571 array of vertical obstacles. *J Nonnewton Fluid Mech* 257:59–70.  
572 <https://doi.org/10.1016/j.jnnfm.2018.04.001>
- 573 Bernabeu N, Saramito P, Smutek C (2016) Modelling lava flow advance using a shallow-depth ap-  
574 proximation for three-dimensional cooling of viscoplastic flows. *Geol Soc Lond Spec Publ* 426:409–  
575 423. <https://doi.org/10.1144/SP426.27>
- 576 Carveni P, Mele G, Benfatto S, Imposa S, Puntillo MS (2011) Lava trees and tree molds ( B cannon  
577 stones ^ ) of Mt. Etna. 633–638. <https://doi.org/10.1007/s00445-011-0446-3>
- 578 Cashman KV, Thornber C, Kauahikaua JP (1999) Cooling and crystalli- zation of lava in open chan-  
579 nels, and the transition of pāhoehoe lava to ‘a’ā. *Bull Volcanol* 61:306–323. <https://doi.org/10.1007/s004450050299>  
580

- 581 Castruccio A, Contreras MA (2016) The influence of effusion rate and rheology on lava flow dyna-  
582 mics and morphology: a case study from the 1971 and 1988-1990 eruptions at Villarrica and Lonqui-  
583 may vol- canoes, Southern Andes of Chile. *J Volcanol Geotherm Res* 327: 469–483.  
584 <https://doi.org/10.1016/j.jvolgeores.2016.09.015>
- 585 Chevrel MO, Harris AJL, James MR, Calabrò L, Gurioli L, Pinkerton H (2018) The viscosity of  
586 pahoehoe lava: in situ syn-eruptive measure- ments from Kilauea, Hawaii. *Earth Planet Sci Lett*  
587 493:161–171. <https://doi.org/10.1016/j.epsl.2018.04.028>
- 588 Chevrel MO, Platz T, Hauber E, Baratoux D, Lavallée Y, Dingwell DB (2013) Lava flow rheology: a  
589 comparison of morphological and petrological methods. *Earth Planet Sci Lett* 384:102–120. <https://doi.org/10.1016/j.epsl.2013.09.022>
- 591 Chirico GD, Favalli M, Papale P, Boschi E, Pareschi MT, Mamou-Mani A (2009) Lava flow hazard at  
592 Nyiragongo volcano, DRC 2 Hazard reduction in urban areas. *Bull Volcanol* 71:375–387.  
593 [https://doi.org/ 10.1007/s00445-008-0232-z](https://doi.org/10.1007/s00445-008-0232-z)
- 594 Crisp J, Baloga S (1994) Influence of crystallization and entrainment of cooler material on the empla-  
595 cement of basaltic ‘a’a lava flows. *J Geophys Res* 99:11,819–11,831. [https://doi.org/10.1029/](https://doi.org/10.1029/94JB00134)  
596 [94JB00134](https://doi.org/10.1029/94JB00134)
- 597 Crisp J, Cashman KV, Bonini JA, Hougén SB, Pieri DC (1994) Crystallization history of the 1984  
598 Mauna Loa lava flow. *J Geophys Res* 99:7177–7198. <https://doi.org/10.1029/93JB02973>
- 599 Dietterich HR, Cashman KV (2014) Channel networks within lava flows: formation, evolution, and  
600 implications for flow behavior. *J Geophys Res Earth Surf* 119:1704–1724. [https://doi.org/10.1002/](https://doi.org/10.1002/2014JF003103)  
601 [2014JF003103](https://doi.org/10.1002/2014JF003103)
- 602 Dietterich HR, Cashman KV, Rust AC, Lev E (2015) Diverting lava flows in the lab. *Nat Geosci* 8:8–  
603 10. <https://doi.org/10.1038/ngeo2470>
- 604 Dragoni M, Tallarico A (1994) The effect of crystallization on the rheol- ogy and dynamics of lava  
605 flows. *J Volcanol Geotherm Res* 59:241– 252. [https://doi.org/10.1016/0377-0273\(94\)90098-1](https://doi.org/10.1016/0377-0273(94)90098-1)
- 606 Finch R (1931) Lava tree casts and tree molds. *Geol Soc Am Bull* 442: 299
- 607 Fiske RS, Koyanagi RY (1968) The December 1965 eruption of Kilauea Volcano, Hawaii. *US Geol*  
608 *Surv Prof Pap* 607:21
- 609 Garel F, Kaminski E, Tait S, Limare A (2014) An analogue study of the influence of solidification on  
610 the advance and surface thermal sig- nature of lava flows. *Earth Planet Sci Lett* 396:46–55. [https://doi.](https://doi.org/10.1016/j.epsl.2014.03.061)  
611 [org/10.1016/j.epsl.2014.03.061](https://doi.org/10.1016/j.epsl.2014.03.061)
- 612 Giordano D, Russell JK, Dingwell DB (2008) Viscosity of magmatic liquids: a model. *Earth Planet*  
613 *Sci Lett* 271:123–134. <https://doi.org/10.1016/j.epsl.2008.03.038>
- 614 Glatzer H (1974) Spectacular show at summit. In: *Hawaii Trib Her.* 20 July 1974. p. 5
- 615 Guest JE, Kilburn CRJ, Pinkerton H, Duncan A (1987) The evolution of flow fields: observations of  
616 the 1981 and 1983 eruptions of Mount Etna, Sicily. *Bull Volcanol* 49:527–540.  
617 [https://doi.org/10.1007/ BF01080447](https://doi.org/10.1007/BF01080447)
- 618 Guilbaud MN, Blake S, Thordarson T, Self S (2007) Role of Syn-eruptive cooling and degassing on  
619 textures of lavas from the AD 1783-1784 Laki eruption, South Iceland. *J Petrol* 48:1265–1294.  
620 [https://doi.org/ 10.1093/petrology/egm017](https://doi.org/10.1093/petrology/egm017)

- 621 Harris AJL, Rowland SK (2015) Lava flows and rheology. *Encycl Volcanoes*, 2nd Ed Eds Sigurdsson  
622 H, Hought B, McNutt SR, Rymer H, Styx J
- 623 Harris AJL, Rowland SK (2001) FLOWGO: a kinematic thermo- rheological model for lava flowing  
624 in a channel. *Bull Volcanol* 63: 20–44. <https://doi.org/10.1007/s004450000120>
- 625 Harris AJL, Rowland SK (2009) Effusion rate controls on lava flow length and the role of heat loss: a  
626 review. *Leg Georg PL Walker, Spec Publ IAVCEI Eds Hoskuldsson A, Thordarson T, Larsen G, Self*  
627 *S, Rowl S Geol Soc London* 2:33–51
- 628 Harris AJL, Villeneuve N, Di Muro A et al (2017) Effusive crises at Piton de la Fournaise 2014-2015:  
629 a review of a multi-national response model. *J Appl Volcanol* 6:11. [https://doi.org/10.1186/s13617-](https://doi.org/10.1186/s13617-017-0062-9)  
630 [017- 0062-9](https://doi.org/10.1186/s13617-017-0062-9)
- 631 Hazlett RW (1993) Geological field guide at Kilauea Volcano. Hawaii Natural History Association,  
632 Honolulu, Hawaii, 127 p.
- 633 Helz RT, Thornber CR (1987) Geothermometry of Kilauea Iki lava lake, Hawaii. *Bull Volcanol*  
634 49:651–668. [https://doi.org/10.1007/ BF01080357](https://doi.org/10.1007/BF01080357)
- 635 Heslop SE, Wilson L, Pinkerton H, Head JW (1989) Dynamics of a confined lava flow on Kilauea  
636 Volcano, Hawaii. *Bull Volcanol* 51: 415–432. <https://doi.org/10.1007/BF01078809>
- 637 Honda T (1998) Physico-chemical explanation for remeleting process of inner surface wall of Tainai  
638 tree molds located on the flank of Mt. Fuji. *J Speleol Soc Japan* 23:29–38. [https://ci.nii.ac.jp/naid/  
639 10027009711/en/](https://ci.nii.ac.jp/naid/10027009711/en/)
- 640 Houghton BF, Wilson CJN (1989) A vesicularity index for pyroclastic deposits. *Bull Volcanol*  
641 51:451–462. [https://doi.org/10.1007/ BF01078811](https://doi.org/10.1007/BF01078811)
- 642 Hulme G (1974) The interpretation of lava flow morphology. *Geophys J R Astron Soc* 39:361–383.  
643 [https://doi.org/10.1111/j.1365-246X. 1974.tb05460.x](https://doi.org/10.1111/j.1365-246X.1974.tb05460.x)
- 644 Jaggar TA (1945) Volcanoes declare war: logistics and strategy of Pacific volcano science. Honolulu,  
645 Hawaii. Paradise of the Pacific, Ltd., 166 p
- 646 James MR, Pinkerton H, Robson S (2007) Image-based measurement of flux variation in distal regions  
647 of active lava flows. *Geochem. Geophys. Geosys.* 8, Q03006. [https://doi.org/10.1029/ 2006GC001448](https://doi.org/10.1029/2006GC001448)
- 648 Jeffreys H (1925) The flow of water in an inclined channel of rectangular section. *Philos Mag serie*  
649 6(4):293,793–293,807
- 650 Jones TJ, Llewellyn EW, Houghton BF, Brown RJ (2017) Proximal lava drainage controls on basaltic  
651 fissure eruption dynamics. *Bull Volcanol* 79:81. <https://doi.org/10.1007/s00445-017-1164-2>
- 652 Kawabata E, Cronin SJ, Bebbington MS, Moufti MRH, El-Masry N, Wang T (2015) Identifying mul-  
653 tiple eruption phases from a com- pound tephra blanket: an example of the AD1256 Al-Madinah erup-  
654 tion, Saudi Arabia. *Bull Volcanol* 77:6. [https://doi.org/10.1007/ s00445-014-0890-y](https://doi.org/10.1007/s00445-014-0890-y)
- 655 Kelfoun K, Vargas SV (2016) VolcFlow capabilities and potential devel- opment for the simulation of  
656 lava flows. In: Harris AJL, De Groot T, Garel F, Carn SA (eds) *Detecting, Modelling and Respon-*  
657 *ding to Effusive Eruptions*. Geological Society, London, pp 337–343
- 658 Keszthelyi L (1995) Measurements of the cooling at the base of pahoehoe flows. *Geophys Res Lett*  
659 22:2195–2198. [https://doi.org/10.1029/ 95GL01812](https://doi.org/10.1029/95GL01812)

- 660 Keszthelyi L, Self S (1998) Some physical requirements for the emplacement of long basaltic lava  
661 flows. *J Geophys Res B* 11:27,447–27, 464. <https://doi.org/10.1029/98JB00606>
- 662 Kolzenburg S, Giordano D, Thordarson T, Hoskuldsson A, Dingwell DB (2017) The rheological evolution of the 2014/2015 eruption at Holuhraun, Central Iceland. *Bull Volcanol* 79:45. <https://doi.org/10.1007/s00445-017-1128-6>
- 663  
664
- 665 Kuntz MA, Spiker EC, Rubin M, Champion DE, Lefebvre RH (1986) Radiocarbon studies of latest  
666 Pleistocene and Holocene lava flows of the Snake River Plain, Idaho: data, lessons, interpretations.  
667 *Quat Res* 25:163–176. [https://doi.org/10.1016/0033-5894\(86\)90054-2](https://doi.org/10.1016/0033-5894(86)90054-2)
- 668 Lincoln NK (2009) *Amy Greenwell Garden Ethnobotanical Guide to Native Hawaiian plants & Polynesian-introduced plants*. Bishop museum press, Honolulu, Hawaii, p 135
- 669
- 670 Lipman PW, Banks NG (1987) Aa flow dynamics, Mauna Loa 1984. *US Geol Surv Prof Pap*  
671 1350:1527–1567
- 672 Llewellyn EW, Manga M (2005) Bubble suspension rheology and implications for conduit flow. *J*  
673 *Volcanol Geotherm Res* 143:205– 217. <https://doi.org/10.1016/j.jvolgeores.2004.09.018>
- 674 Lockwood JP, Hazlett RW (2010) *Volcanoes global perspectives*. Wiley- Blackwell. Chichester, United  
675 Kingdom, p 539
- 676 Lockwood JP, Tilling RI, Holcomb RT, Klein F, Okamura AT, Peterson DW (1999) Magma migration and resupply during the 1974 summit eruptions of Kilauea volcano, Hawai'i. *US Geol Surv Prof Pap* 1613(37)
- 677  
678
- 679 Lockwood JP, Williams IS (1978) Lava trees and tree moulds as indicators of lava flow direction.  
680 *Geol. Mag.* 115:69–74. <https://doi.org/10.1017/S0016756800041005>
- 681 MacDonald GA, Abbott AT, Peterson FL (1983) *Volcanoes and the sea - The geology of Hawaii*.  
682 University of Hawaii Press, Honolulu, Hawaii, p 517
- 683 Mader HM, Llewellyn EW, Mueller SP (2013) The rheology of two-phase magmas: a review and analysis. *J Volcanol Geotherm Res* 257:135– 158. <https://doi.org/10.1016/j.jvolgeores.2013.02.014>
- 684
- 685 Malin MC (1980) Lengths of Hawaiian lava flows. *Geology* 8:306– 308. [https://doi.org/10.1130/0091-7613\(1980\)8<306:LOHLF>2.0.CO;2](https://doi.org/10.1130/0091-7613(1980)8<306:LOHLF>2.0.CO;2)
- 686
- 687 Maron SH, Pierce PE (1956) Application of Ree-Eyring generalized flow theory to suspensions of  
688 spherical particles. *J Colloid Sci* 11:80–95. [https://doi.org/10.1016/0095-8522\(56\)90023-X](https://doi.org/10.1016/0095-8522(56)90023-X)
- 689 Merlin M (1995) *Hawaiian forest plants*. Pacific guide books, Honolulu, Hawaii. 80 p.
- 690 Moore HJ (1987) Preliminary estimates of the rheological properties of 1984 Mauna Loa Lava. *US Geol Surv Prof Pap* 1350(99):1569– 1588
- 691
- 692 Moore HJ, Kachadoorian R (1980) Estimates of lava-flow velocities using lava trees. *Reports Plan Geol Prog* 1979–1980:201–203  
693 Moore JG, Richter DH (1962) Lava tree molds of the September 1961  
694 eruption, Kilauea volcano, Hawaii. *Geol Soc Am Bull* 73:1153– 1158. [https://doi.org/10.1130/0016-7606\(1962\)73\[1153:LTMOTS\]2.0.CO;2](https://doi.org/10.1130/0016-7606(1962)73[1153:LTMOTS]2.0.CO;2)
- 695
- 696 Mougini-mark PJ, Garbeil H (2005) Quality of TOPSAR topographic data for volcanology studies at  
697 Kilauea Volcano, Hawaii: an assessment using airborne lidar data. *Remote Sensing of Environment*

- 698 96: 149–164. <https://doi.org/10.1016/j.rse.2005.01.017>
- 699 Mueller S, Llewellyn EW, Mader HM (2010) The rheology of suspen-  
700 sions of solid particles. *Philos Trans R Soc Lond A* 466:1201–1228. <https://doi.org/10.1098/rspa.2009.0445>
- 701 Nichols RL (1939) Superficial banding and shark’s-tooth projections in the cracks of basaltic lava.  
702 *Amer* 237:188–194. <https://doi.org/10.2475/ajs.237.3.188>
- 703 Parcheta CE, Houghton BF, Swanson DA (2012) Hawaiian fissure foun-  
704 tains 1: decoding deposits—  
705 episode 1 of the 1969–1974 Mauna Ulu eruption. *Bull Volcanol* 74:1729–1743.  
<https://doi.org/10.1007/s00445-012-0621-1>
- 706 Peterson DW, Tilling RI (1980) Transition of basaltic lava from pāhoehoe to ‘a‘ā, Kilauea volcano,  
707 Hawaii: field observations and key factors. *J Volcanol Geotherm Res* 7:271–293.  
708 [https://doi.org/10.1016/0377-0273\(80\)90033-5](https://doi.org/10.1016/0377-0273(80)90033-5)
- 709 Pinkerton H, Stevenson RJ (1992) Methods of determining the rheolog-  
710 ical properties of magmas at  
711 sub-liquidus temperatures. *J Volcanol Geotherm Res* 53:47–66. [https://doi.org/10.1016/0377-0273\(92\)90073-M](https://doi.org/10.1016/0377-0273(92)90073-M)
- 712 Pinkerton H, Wilson L (1988) The lengths of lava flows. *Lunar Planet Sci. Abstr.*, XIX. pp 937–938
- 713 Pinkerton H, Wilson L (1994) Factor controlling the lengths of channel-  
714 fed lava flows. *Bull Volcanol* 6:108–120. <https://doi.org/10.1007/BF00304106>
- 715 Pratt L, Gon SM III (1998) Terrestrial ecosystems. In: *Atlas of Hawaii*. University of Hawaii Press,  
716 Honolulu, Hawaii, pp 121–129
- 717 Rhéty M, Harris A, Villeneuve N, Gurioli L, Médard E, Chevrel O, Bachélery P (2017) A comparison  
718 of cooling-limited and volume-limited flow systems: Examples from channels in the Piton de la Four-  
719 naise April 2007 lava-flow field, *Geochem Geophys Geosyst* 18  
720 <https://doi.org/10.1002/2017GC006839>
- 721 Riker JM, Cashman KV, Kauahikaua JP, Montierth CM (2009) The length of channelised lava flows:  
722 insight from the 1859 eruption of Mauna Loa Volcano, Hawaii. *J Volcanol Geotherm Res* 183:139–  
723 156. <https://doi.org/10.1016/j.jvolgeores.2009.03.002>
- 724 Robert B, Harris A, Gurioli G, Medard E, Sehlke A, Whittington A (2014) Textural and rheological  
725 evolution of basalt flowing down a lava channel. *Bull Volcanol* 76:824. <https://doi.org/10.1007/s00445-014-0824-8>
- 726
- 727 Rumpf ME, Lev E, Wysocki R (2018) The influence of topographic roughness on lava flow emplace-  
728 ment. *Bull Volcanol* 80:63. <https://doi.org/10.1007/s00445-018-1238-9>
- 729
- 729 Sakimoto SEH, Gregg TKP (2001) Channeled flow: analytic solutions, laboratory experiments, and  
730 applications to lava flows. *J Geophys Res* 106:8629–8644. <https://doi.org/10.1029/2000JB900384>
- 731
- 731 Scifoni S, Coltelli M, Marsella M, Proietti C, Napoleoni Q, Vicari A, Del Negro C (2010) Mitigation  
732 of lava flow invasion hazard through optimized barrier configuration aided by numerical simulation:  
733 the case of the 2001 Etna eruption. *J Volcanol Geotherm Res* 192:16–26.  
734 <https://doi.org/10.1016/j.jvolgeores.2010.02.002>
- 735
- 735 Searle EJ (1958) A note on the formation of native iron and other effects associated with contact of  
736 basalt and carbonized wood at Auckland, New Zealand. *New Zeal J Geol Geophys* 1:451–458

- 737 Sehlke A, Whittington A, Robert B, Harris AJL, Gurioli L, Médard E (2014) Pahoehoe to ‘a’ transition of Hawaiian lavas: an experimental study. *Bull Volcanol* 76:876. [https://doi.org/10.1007/s00445-](https://doi.org/10.1007/s00445-014-0876-9)  
738 [014-0876-9](https://doi.org/10.1007/s00445-014-0876-9)  
739
- 740 Shea T, Houghton BF, Gurioli L, Cashman KV, Hammer JE, Hobden BJ (2010) Textural studies of  
741 vesicles in volcanic rocks: an integrated methodology. *J Volcanol Geotherm Res* 190:271–289.  
742 <https://doi.org/10.1016/j.jvolgeores.2009.12.003>
- 743 Smathers GA, Mueller-Dombois D (2007) Hawai’i, the fires of life. Mutual Publishing, Honolulu, p  
744 141
- 745 Soule SA, Cashman KV, Kauahikaua JP (2004) Examining flow emplacement through the surface  
746 morphology of three rapidly emplaced, solidified lava flows, Kīlauea Volcano, Hawai’i. *Bull Volcanol*  
747 66:1–14. <https://doi.org/10.1007/s00445-003-0291-0>
- 748 Swanson DA (1973) Pāhoehoe flows from the 1969-1971 Mauna Ulu eruption, Kīlauea volcano, Ha-  
749 waii. *Bull Geol Soc Am* 84:615–626. <https://doi.org/10.1130/0016-7606>
- 750 Thivet S (2016) Caractérisation magmatique du système superficiel du Piton de la Fournaise à travers  
751 l’étude des produits de l’éruption de Juillet 2015. Université Clermont-Auvergne
- 752 Van Wagner CE (1967) Calculations on forest fire spread by flame radiation. Government of Canada,  
753 Department of Forestry and Rural Development, Petawawa Forest Experiment Station, Chalk River,  
754 Ontario. Departmental publication 1185. 18 p.
- 755 Wilson L, Head JW (1994) Mars review and analysis of volcanic eruption theory and relationships to  
756 observed landforms. *Rev Geophys* 32: 221–263. <https://doi.org/10.1029/94RG01113>

757

## 758 **Figure captions**

759 Figure 1: Lava-tree formation (modified from Lockwood and Hazlett, 2010). a) Pristine forest  
760 contains trees of various sizes and heights. b) When lava is in contact with air or with cooler  
761 surfaces (ground and vertical obstacles like trees) it rapidly quenches and forms a chilled crust  
762 (black) surrounding the hot, fluid interior (orange), and vegetation dries and burns. c) Lava  
763 drains away, causing the subsidence of the flow surface and leaving behind standing lava-tree  
764 casts and a dead forest. Measured lava tree dimensions are given in c.

765

766 Figure 2: Map of the south-eastern July 1974 lava flow showing the studied unit and location  
767 of samples and lava-trees (background of GoogleEarth image © 2018 DigitalGlobe). Inset  
768 map showing the location of the studied lava flow, modified from Lockwood et al. (1999).

769 *Lava-trees* (black points) were located based on aerial photography, TOPSAR images and  
770 ground truthing. “*Sampled lava-trees*” indicates location where rock samples were taken (T1 to  
771 T10; Table 1); “V” is the location of a sample taken at the vent.

772

773 Figure 3: Sampling methodology along the lava flow and thin section positions on lava-tree  
774 casts. Yellow dots indicate the presence of glassy matrix in the thin section.

775

776 Figure 4: Sampling of a single lava-tree (T10). From left to right: photo of T10 with location  
777 of samples) from top to bottom (labeled from A to G); sketch of the main features and dimen-  
778 sions, and variation of temperature (*circles*) and crystallinity (*squares*) as function the height.

779

780 Figure 5: Evolution of width (*empty circles*) and thickness (*full circles*) of the studied lava  
781 flow as function of distance from the vent. Vertical dashed lines and numbers outline the five  
782 zones of the lava flow morphology: 1) near-vent pāhoehoe sheet flow; 2) proximal channel  
783 area with multiple incipient channels; 3) well-formed channel that divided in two main chan-  
784 nels; 4) coalescence into a single broad channel made of ‘a‘ā and pāhoehoe slabs between  
785 broad initial levées; 5) dispersed ‘a‘ā flow.

786

787 Figure 6: Number of lava-trees per hectare and percentage of lava type (pāhoehoe vs. ‘a‘ā)  
788 down flow.

789

790 Figure 7: Examples of lava-tree morphologies: a) lava-trees “en bouquet” near the vent; b)  
791 vertical closed lava-tree; c) open lava-tree with remaining dead tree; d) scratching of the plas-  
792 tic outer surface of the cast causing striations and tension gashes; e) uptilted pāhoehoe slabs

793 remaining in-place surrounding the base of a lava-tree, forming a dome like structure; f) barri-  
794 er made by accretion around and between two lava-trees.

795

796 Figure 8: SEM images of the matrix crystallization down flow.

797

798 Figure 9: Down flow variations in the temperature obtained from the glassy matrix on the lava  
799 side (*open circles*) and on the tree side (*full circles*) of each sample, and crystal content in-  
800 cluding phenocrysts + microlites (*squares*). Linear regression lines indicate 10°C/km on the  
801 lava side ( $R^2=0.78$ ) and 4 °C/km on the tree side ( $R^2=0.60$ ). The temperature gradient from  
802 Soule et al. (2004) is also reported for comparison (7 °C/km  $R^2=0.71$ ). The linear regression  
803 for the crystallinity indicates 16.2 vol.% / km ( $R^2=0.9$ ).

804

805 Figure 10: a) Down flow variation of the vesicularity derived from density; b) Cumulative  
806 vesicle number density plot considering the vesicle number density per volume in  $\text{mm}^{-3}$  ( $N_v$ )  
807 with diameter greater than L (the equivalent diameter of the vesicle).

808

809 Figure 11: a) Down flow variation in the velocity (*diamonds*) and viscosity (*crosses*). The  
810 *black diamonds* are our calculations and the *open diamonds* are the estimations given by  
811 Moore and Kachadorian (1980); b) Velocity (*diamonds*) and viscosity (*crosses*) calculated  
812 with flow depth around T10.

813

814 Figure 12: Conceptual model for the interaction of lava and trees depending on the lava type.

815

## 816 **Table captions**

817 Table 1: Sample location and description

818 Table 2: Textural analyses down the flow

819 Table 3: Textural analyses and viscosity estimation along a single tree (T10)

820 Table 4: Viscosity and velocity estimation along the flow

821 Table 5: Reconstruction of the effusion rate history

822

Figure 1

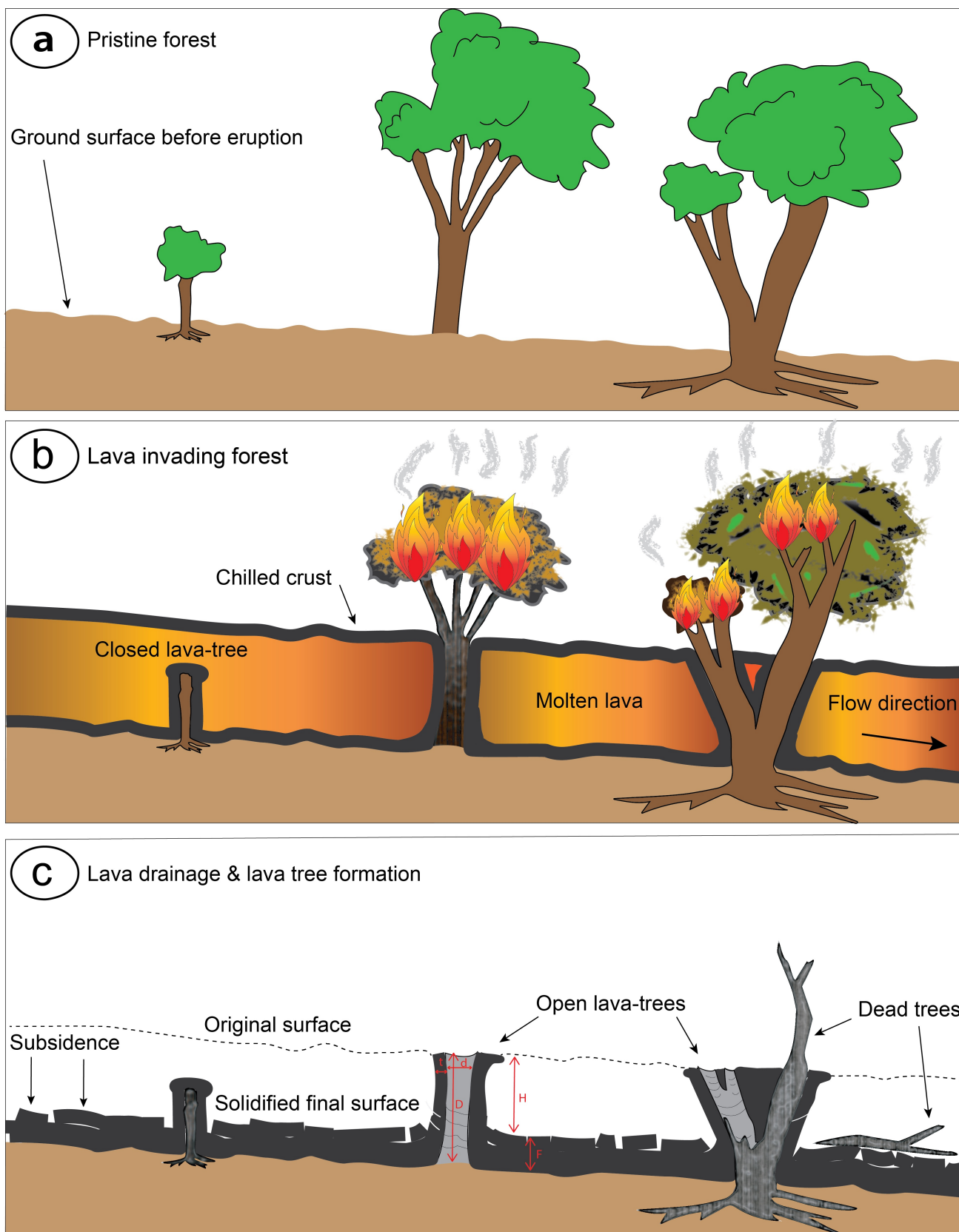


Figure 2

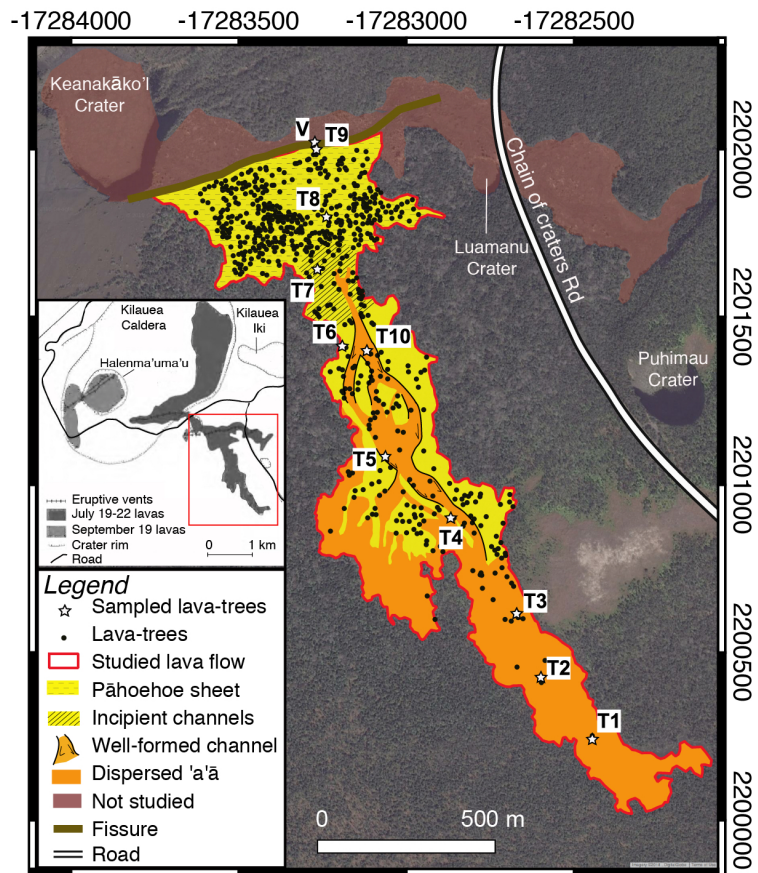


Figure 3

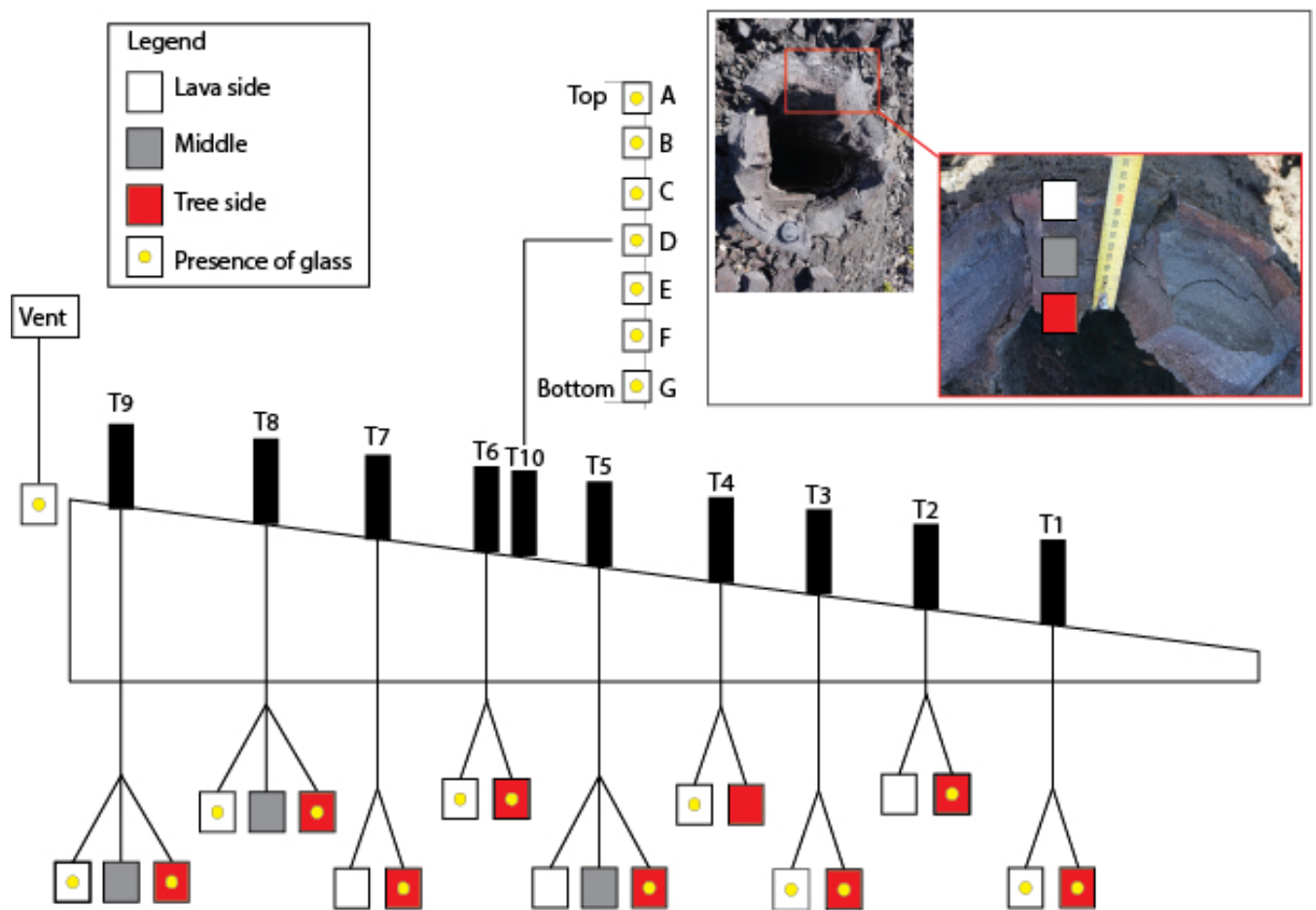


Figure 4

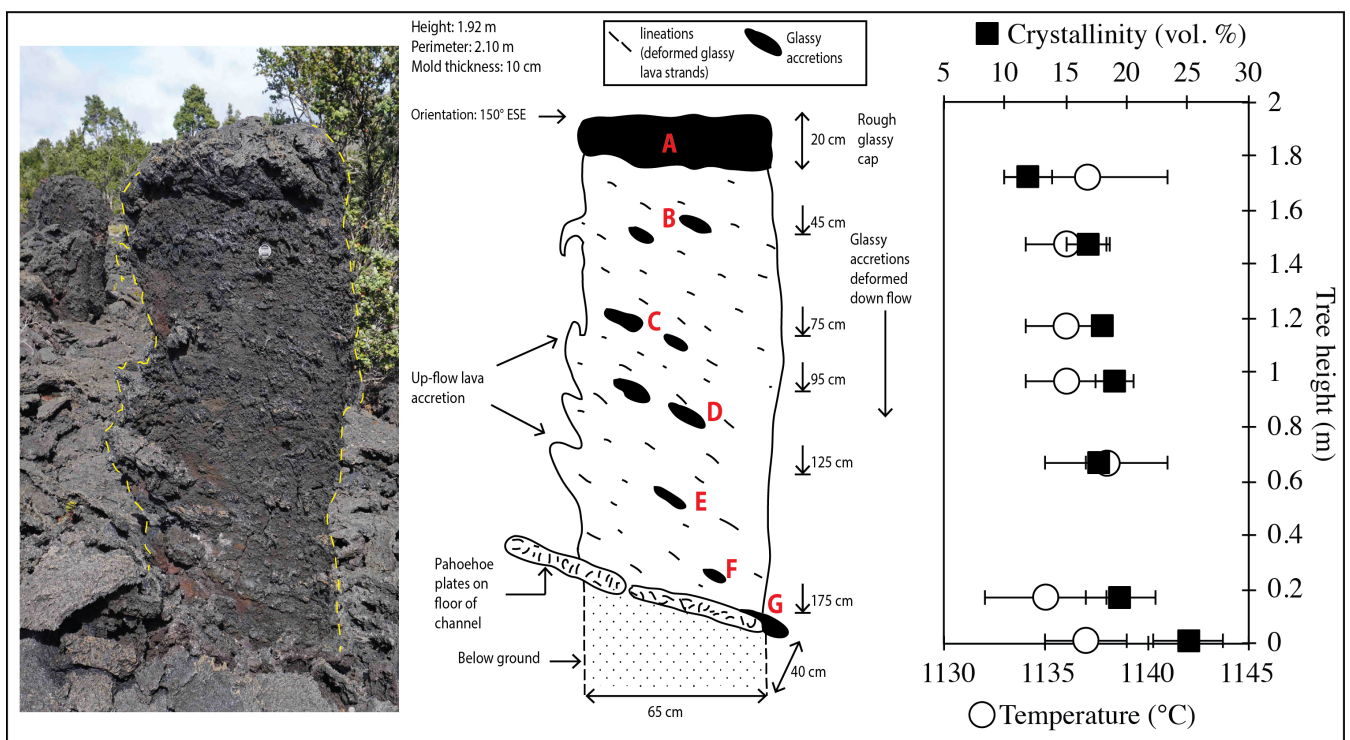


Figure 5

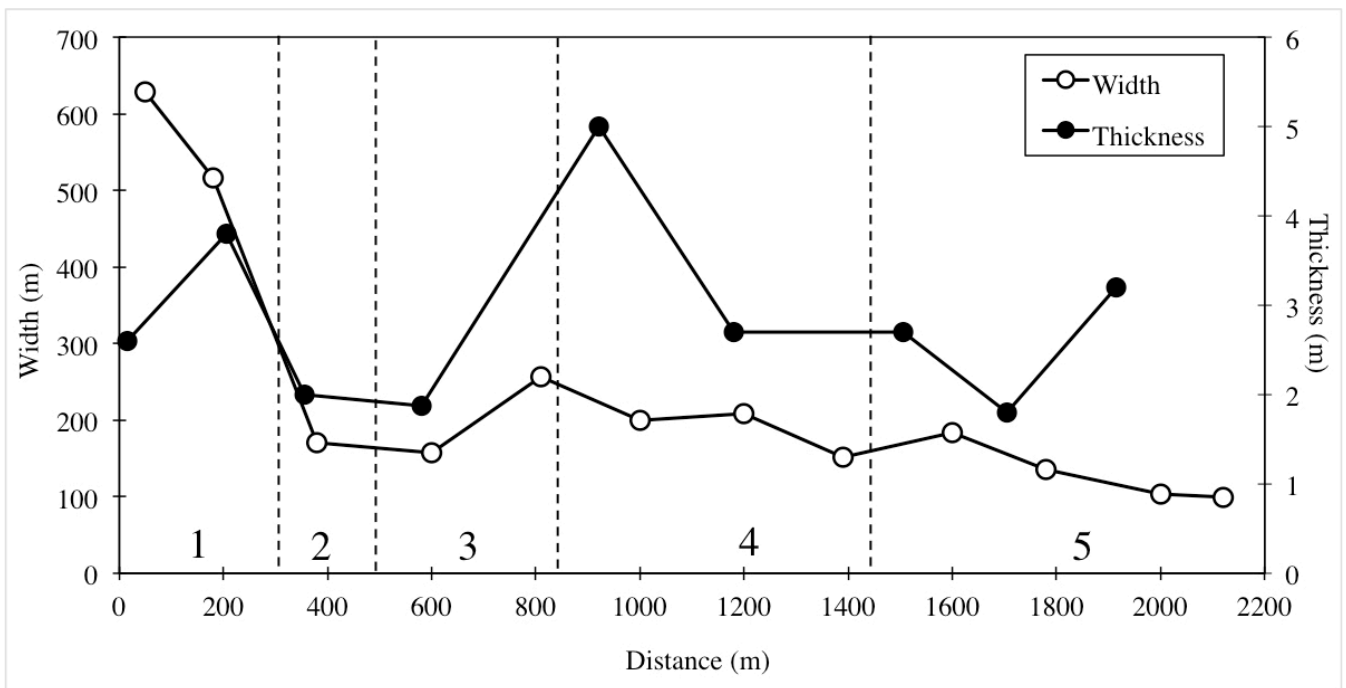


Figure 6

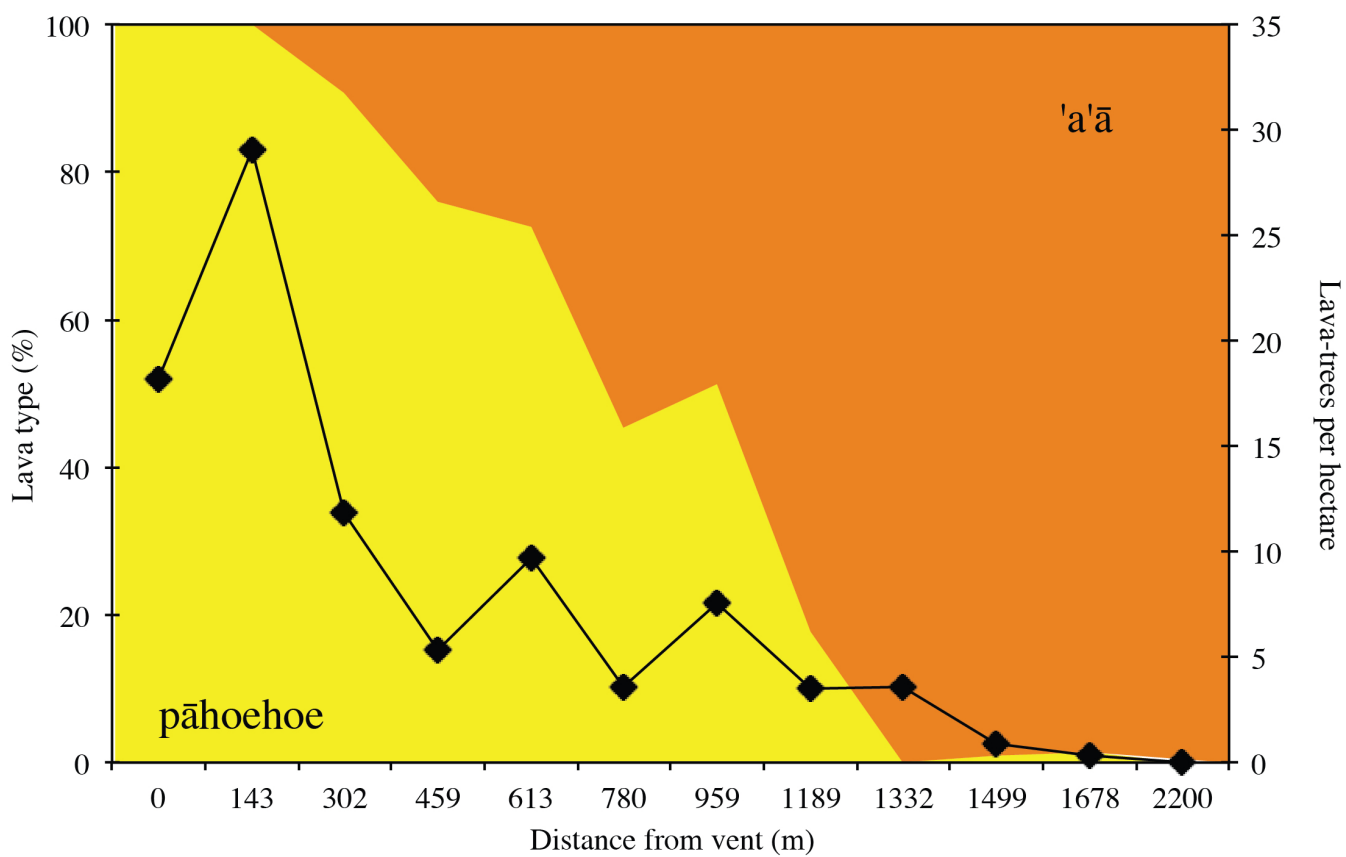
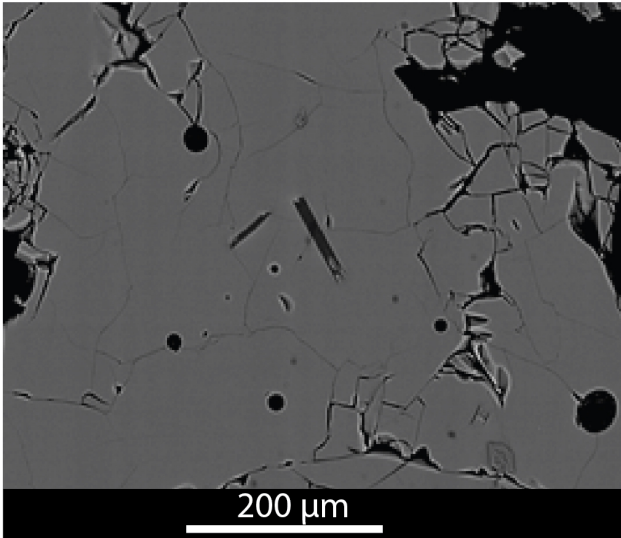


Figure 7

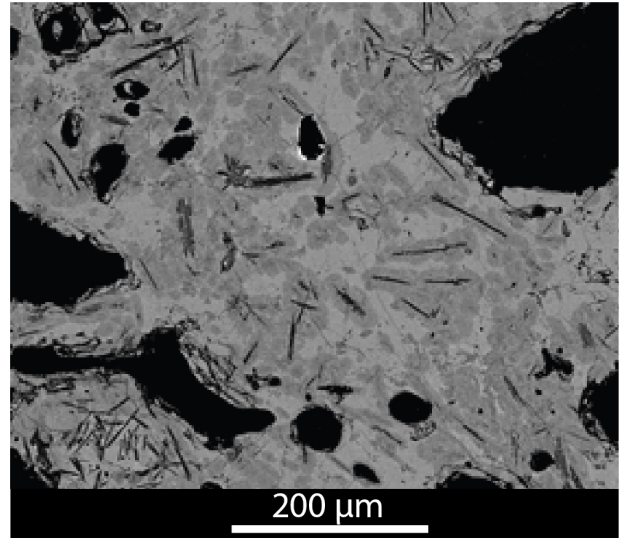


**Figure 8**

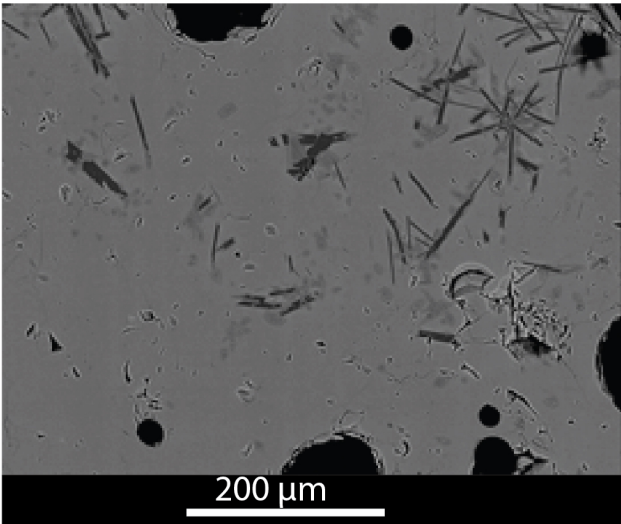
**T9-T** Distance : 15 m  
Microlites :  $0.6 \pm 0.2$  %



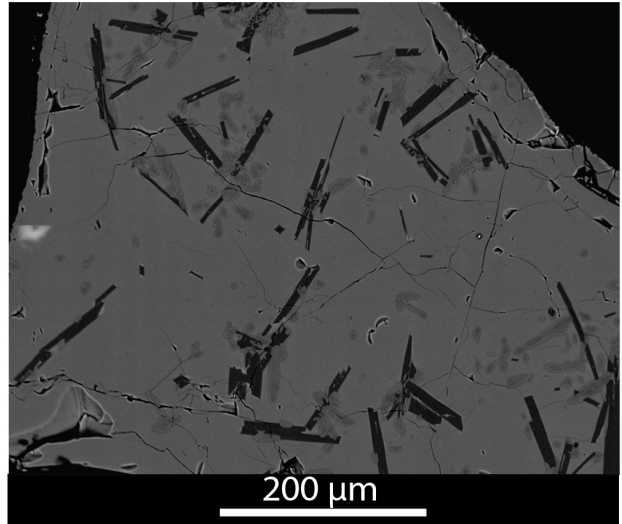
**T8-T** Distance : 205 m  
Microlites :  $5.6 \pm 1.5$  %



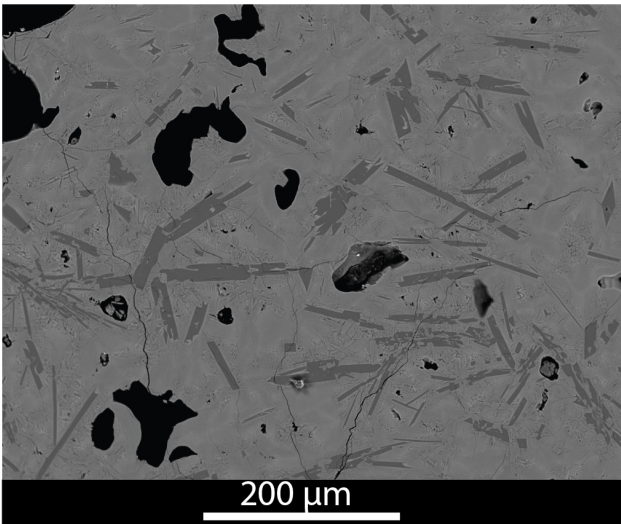
**T7-T** Distance : 355 m  
Microlites :  $13.4 \pm 4.1$  %



**T10-T** Distance : 600 m  
Microlites :  $15.3 \pm 6.8$  %



**T5-T** Distance : 920 m  
Microlites :  $16.9 \pm 7.2$  %



**T1-T** Distance : 1915 m  
Microlites :  $33.1 \pm 3.0$  %

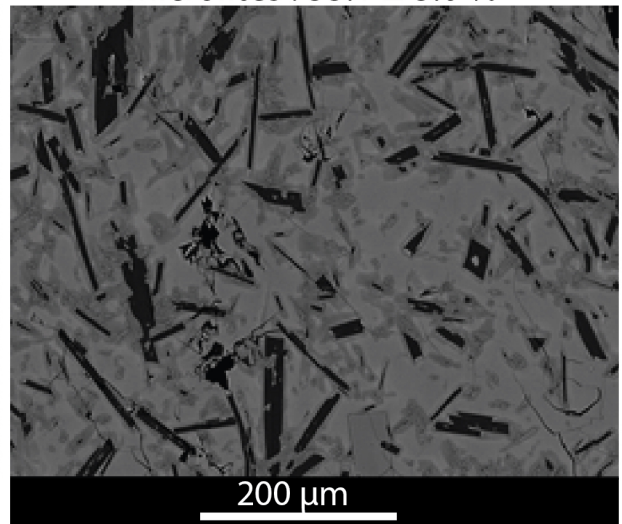


Figure 9

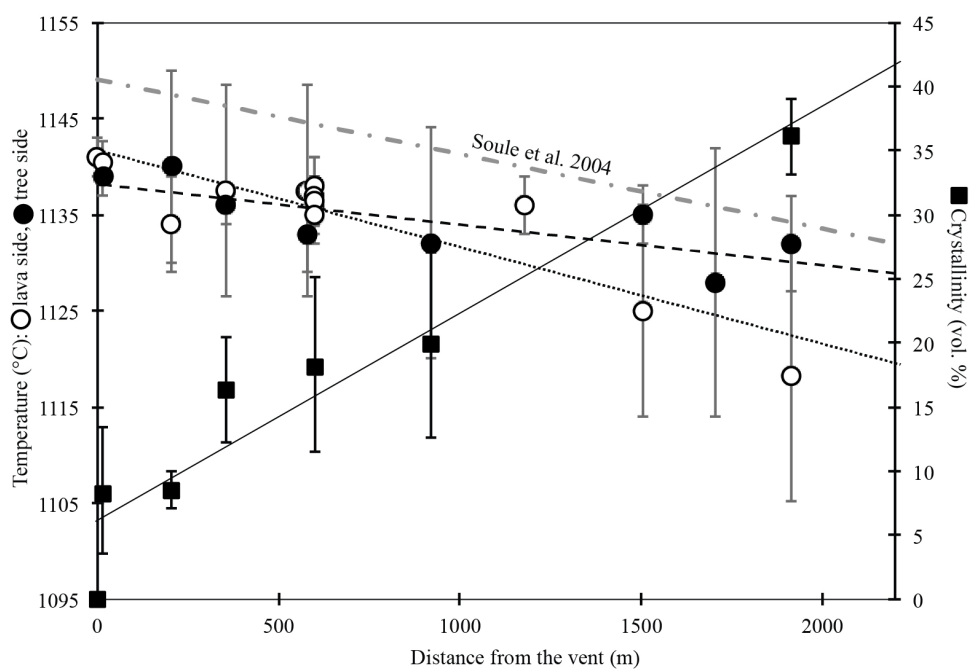


Figure 10

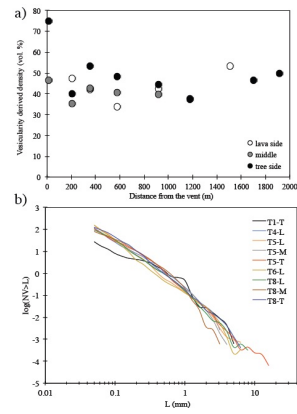
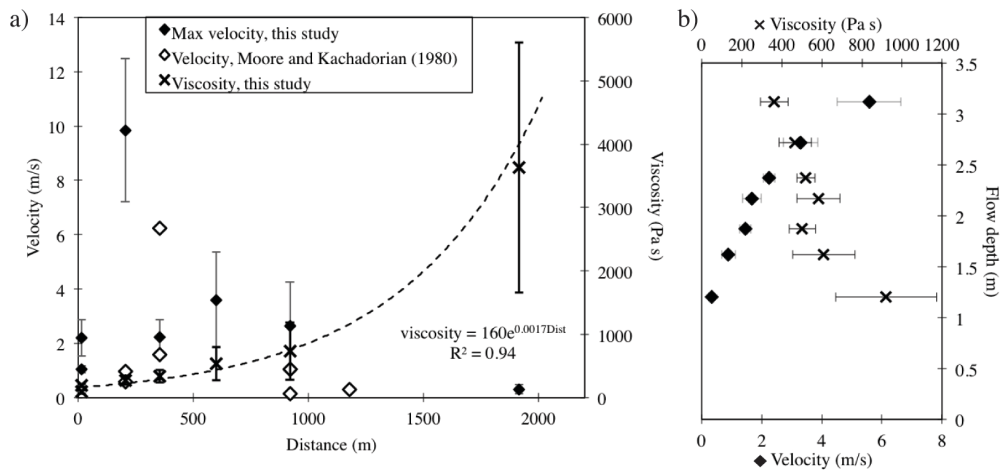
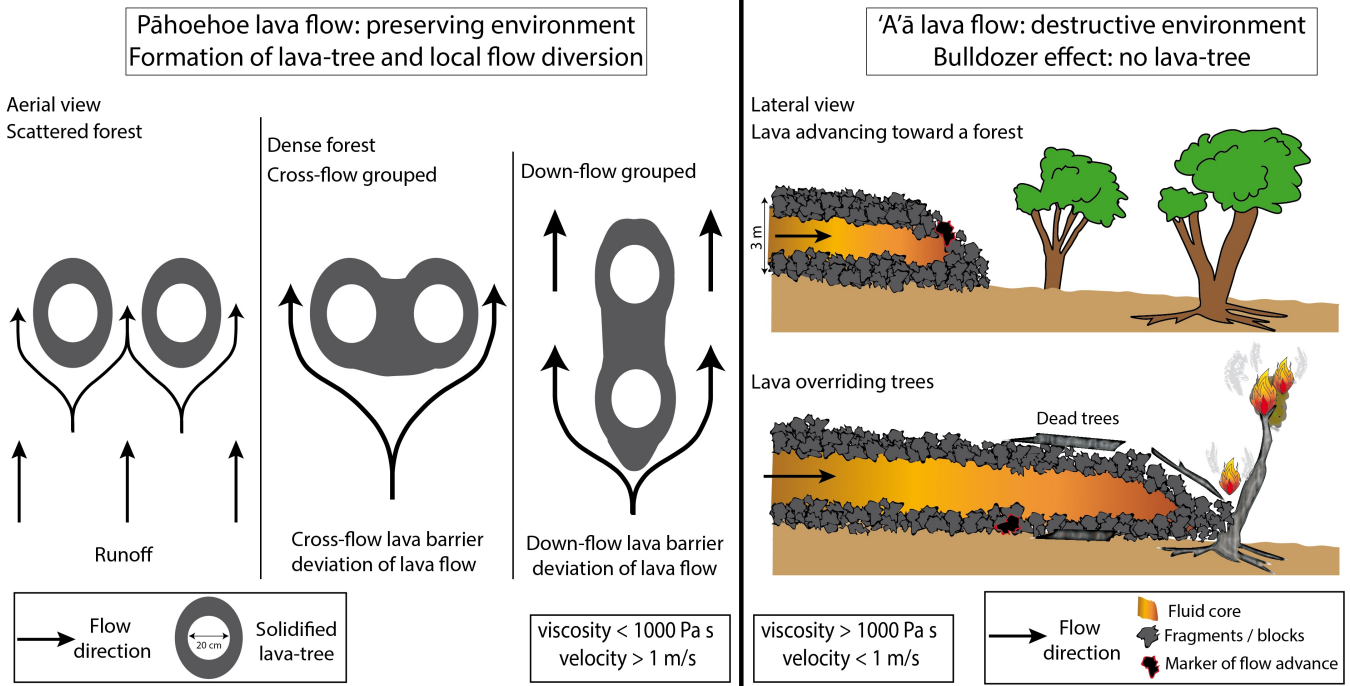


Figure 11



**Figure 12**



**Table 1**

Sample	GPS coordinates		Distance from vent (m)	Height of the lava-tree (m)	Description
	Latitude (N)	Longitude (W)			
Vent	19°23'57.8710"	155°15'29.6680"	0	--	Glassy spatter t vent
T9	19°23'57.3504"	155°15'29.5245"	15	2.6	Near the vent, sheet pahoehoe
T8	19°23'51.2160"	155°15'28.5489"	205	3.8	Sheet pahoehoe zone
T7	19°23'46.4604"	155°15'29.3742"	355	2	Gas-rich zone, shelly pahoehoe
T6	19°23'39.4332"	155°15'27.0157"	580	1.88	Shear zone in the channel, slabby pahoehoe
T10	19°23'39.0408"	155°15'24.6118"	600	1.92	Near T6, edge of the channel
T5	19°23'29.2380"	155°15'23.2431"	920	5	Tree with three trunks, in channel of slabby pahoehoe
T4	19°23'23.8272"	155°15'16.5212"	1180	2.7	Slabby pahoehoe
T3	19°23'14.9604"	155°15'10.4030"	1505	2.7	Slabby pahoehoe to 'a'a lava
T2	19°23'08.8764"	155°15'08.1606"	1705	--	Slabby pahoehoe to 'a'a lava
T1	19°23'04.0596"	155°15'03.2633"	1915	3.2	First lava tree found since the front, essentially 'a'a lava

**Table 2**

Sample	Distance from vent (m)	Number of glass per sample	Temperature (°C)	+/-	Density (kg/m <sup>3</sup> )	vesicularity-derived density (vol. %)	2D vesicularity (vol. %)	Microclite (vol. %)	Total crystal content (vol. %)**	+/-
VENT	0	20	1141	2	--	--	--	--	3	--
T9-L	15	11	1140	2	--	--	--	10.5	13.5	1.6
T9-M	15	--	--	--	1620	46.5	--	--	--	--
T9-T	15	10	1139	2	756	75.1	--	0.6	3.6	0.2
T8-L	205	10	1134	5	1599	47.2	44.4	--	--	--
T8-M	205	--	--	--	1959	35.4	38.4	--	--	--
T8-T	205	30	1140	10	1811	40.2	54.8	5.6	8.6	1.4
T7-L	355	10	1138	11	1757	42.0	--	--	--	--
T7-M	355	--	--	--	1743	42.5	--	--	--	--
T7-T	355	10	1136	2	1416	53.3	--	13.4	16.4	4.1
T6-L	580	10	1138	11	2001	34.0	37.6	-	-	--
T6-M	580	--	--	--	1798	40.7	--	--	--	--
T6-T	580	10	1133	4	1566	48.3	--	--	--	--
T10-L mean	600	--	1136	3	--	--	--	15.3	18.3	6.8
T5-L	920	--	--	--	1749	42.3	40.8	--	--	--
T5-M	920	--	--	--	1821	39.9	39.1	--	--	--
T5-T	920	11	1132	12	1677	44.6	60.4	16.8	19.8	7.2
T4-L	1180	10	1136	3	1887	37.7	44.6	--	--	--
T4-T	1180	--	--	--	1898	37.4	--	--	--	--
T3-L	1505	10	1125	11	1412	53.4	--	--	--	--
T3-T	1505	10	1135	3	1507	50.3	--	--	--	--
T2-L	1705	--	--	--	0	--	--	--	--	--
T2-T	1705	10	1128	14	1626	46.3	--	--	--	--
T1-L	1915	10	1118	13	0	--	--	--	--	--
T1-T	1915	15	1132	5	1522	49.8	54.3	33.1	36.1	3.0

\* Mg-thermometer from 10 glass analyses per sample

\*\* + 3 vol. % of phenocrysts

**Table 3**

Level	Sample	Distance from top (m)	Flow Depth (m)	Temperature (°C) <sup>a</sup>		Melt viscosity (Pa s) <sup>b</sup>		Crystallinity (vol.%) <sup>c</sup>		Relative viscosity crystal effect <sup>d</sup>		Viscosity of three phase mixture (Pa s) <sup>e</sup>		Velocity (m/s) <sup>f</sup>		Effusion Rate (m <sup>3</sup> /s)		
				±	±	±	±	±	±	±	±	±	±					
High-Stand	A	0	3.12	1137	4	481	27	11.9	2.0	1.8	0.6	363	124	5.6	1.9	304	58	
	1	B	0.4	2.72	1137	2	460	22	16.9	1.7	2.4	0.5	467	99	3.3	0.7	157	27
	2	C	0.75	2.37	1136	2	475	14	18.0	0.3	2.6	0.1	520	24	2.2	0.1	93	8
	3	D	0.95	2.17	1136	2	498	28	19.0	1.6	2.7	0.5	583	101	1.7	0.3	64	12
	4	E	1.25	1.87	1138	3	469	19	17.7	1.0	2.5	0.3	502	61	1.4	0.2	47	6
Low-Stand	5	F	1.5	1.62	1135	3	505	29	19.5	2.9	2.8	0.8	610	185	0.9	0.3	25	6
	G	1.75	1.20	1137	2	491	20	25.1	2.9	4.4	1.0	921	213	0.3	0.1	7	2	

<sup>a</sup> Mg-thermometer from 10 glass analyses per sample  
<sup>b</sup> calculated via Giordano et al. 2008  
<sup>c</sup> including phenocrysts and microlites  
<sup>d</sup> considering the crystallinity and calculated via Mader et al. 2014 for phi max =0.48 (r=3.6)  
<sup>e</sup> considering 40±0.1% of deformable bubble via Lewelin and Manga 2005  
<sup>f</sup> Jeffreys equation with slope of 2° and density of 1.82

**Table 4**

Tree	Zone	Distance from vent (m)	Max flow Depth (m)	Final Flow Depth (m)	Slope (°)	Melt viscosity (Pa s) <sup>a</sup>			Viscosity of three phase mixture (Pa s) <sup>b</sup>			Max velocity (m/s) <sup>c</sup>		Min velocity (m/s) <sup>c</sup>	
						±	±	±	±	±	±	±			
T9-T	1: sheet flow	15	2.6	0.9	0.3	471	54	193	23	1.0	0.1	0.1	0.0		
T9-L	1: sheet flow	15	2.6	0.9	0.3	478	41	91	28	2.2	0.7	0.3	0.1		
T8	1: sheet flow	205	3.8	2.4	1.9	441	113	277	74	9.8	2.6	3.9	1.1		
T7	2: proximal channel	355	2.0	0.2	1.9	523	61	338	97	2.2	0.6	0.01	0.0		
T6	3: Medial channel	580	1.9	0.7	2.0	--	--	--	--	--	--	--	--		
T10	3: Medial channel	600	3.1	1.7	2.0	483	164	538	263	3.6	1.8	1.1	0.5		
T5	3: Medial channel	920	5.1	1.7	0.8	678	236	735	457	2.6	1.6	0.3	0.2		
T4	4: Distal channel	1180	2.7	1.4	0.8	--	--	--	--	--	--	--	--		
T3	5: Dispersed flow	1505	2.7	0.6	0.8	--	--	--	--	--	--	--	--		
T2	5: Dispersed flow	1705	1.8	1.8	1.1	--	--	--	--	--	--	--	--		
T1	5: Dispersed flow	1915	3.2	1.2	1.1	702	145	3634	1975	0.3	0.2	0.04	0.02		

<sup>a</sup> calculated via Giordano et al. 2008 using the glass composition and temperature reported in Table 2

<sup>b</sup> considering the crystal content and vesicularity reported in Table 2 and assuming phi max =0.48 (r=3.6) and deformable bubble via Llewelin and Manga 2005

<sup>c</sup> Calculated from Jeffreys equation with a density of 1740 kg/m<sup>3</sup>

**Table 5**

Time (hours)	Effusion Rate (m <sup>3</sup> /s)	Duration (h)	Volume Emplaced (m <sup>3</sup> )
1.8	403	1.8	$2.55 \times 10^6$
2.6	209	0.9	$6.57 \times 10^5$
3.1	124	0.4	$1.95 \times 10^5$
3.3	85	0.2	$6.68 \times 10^4$
3.4	63	0.1	$2.48 \times 10^4$
3.4	34	0.05	$6.64 \times 10^3$
3.5	9	0.03	$8.93 \times 10^2$
Total	280	3.5	$3.5 \times 10^6$